EXPERIMENTAL DESIGN ON HIGH-SPEED SLIDING WEAR

THESIS

Irene D. Liew, Second Lieutenant, USAF

AFIT-ENS-MS-22-M-145

DEPARTMENT OF THE AIR FORCE
AIR UNIVERSITY

AIR FORCE INSTITUTE OF TECHNOLOGY

Wright-Patterson Air Force Base, Ohio

AFIT-ENS-MS-22-M-145

EXPERIMENTAL DESIGN ON HIGH-SPEED SLIDING WEAR

THESIS

Presented to the Faculty

Department of Operational Sciences

Graduate School of Engineering and Management

Air Force Institute of Technology

Air University

Air Education and Training Command

in Partial Fulfillment of the Requirements for the

Degree of Master of Science in Operations Research

Irene D. Liew, M.S.

Second Lieutenant, USAF

March 2022

AFIT-ENS-MS-22-M-145

EXPERIMENTAL DESIGN ON HIGH-SPEED SLIDING WEAR

THESIS

Irene D. Liew, M.S.

Second Lieutenant, USAF

Committee Membership:

Raymond Hill, Ph.D.
Chair

Anthony Palazotto, Ph.D., P.E.
Member

Tony Liu, Captain, Ph.D.
Member

AFIT-ENS-MS-22-M-145

Abstract

The purpose of this research is to develop, conduct, and analyze an experimental design that characterizes wear rates of various materials sliding at high speeds along an AISI 4340 steel rail. This work is in support of Holloman Air Force Base, which is invested in engineering a more wear-resistant rocket slipper for its high-speed test track. This research uses a design of experiments approach to systematically identify and evaluate potential slipper attributes that mitigate wear according to a heat transfer model. Final findings include recommendations of slipper materials that theoretically perform similar to or better than the baseline Vascomax®C300 maraging steel material. Concurrently, this research statistically evaluates the finite element analysis heat transfer model of the Air Force Research Laboratory's pin-on-disc experiment.

Acknowledgements

This research is sponsored by the Air Force Research Laboratory, Aerospace Systems Directorate. I'd like to extend thanks to the team there who supported this research effort, including Dr. Russ Spyker and Laura Walter. Your technical expertise and eagerness to aid my experimentation are much appreciated. This work is in support of the 846th Test Squadron at Holloman AFB. Thank you, Dr. Mike Hooser, for helping to lay the foundation for my approach.

I'd also like to extend a big thanks to my research advisor, Dr. Ray Hill. He has not only provided amazing guidance on the experimentation and modeling of this work, but has guided me through various trials here at AFIT. The other members of my thesis committee, Dr. Anthony Palazotto and Dr. Tony Liu, have provided invaluable insight on the background, mechanics, and mathematics behind this research problem. Thank you Dr. Palazotto for your extensive involvement and wisdom, and Dr. Liu for always being there to give me guidance.

Finally, infinite thanks to my partner for your endless support.

Irene D. Liew

Table of Contents

List of Figures

List of Tables

I. Introduction

1.1 Motivation

This work is in support of Holloman Air Force Base's (AFB) Holloman High Speed Test Track (HHSTT), operated by the United States Air Force's (USAF) 846th Test Squadron. Holloman AFB states that the mission of their high-speed rocket sled tests is to enable critical weapon system development in support of the warfighter. The HHSTT serves as a critical link between laboratory and full-scale flight tests by simulating select portions of the flight environment. This provides an efficient, safe, and cost-effective ground test alternative to developmental flight tests ("846th Test Squadron").

The HHSTT uses sled "slippers" as the interface that attach the rocket sled to the rail on which it slides. The rocket sled configuration and slippers are shown in **Figure 1.1.** Current slippers are composed of maraging 300 alloy steel, commercially known as Vascomax®C300. The rail of the track is composed of AISI 4340 alloy steel. As the rocket slides along the track at high speeds, the slippers experience documented issues with wear due to frictional, thermal, and mechanical properties.

Excessive slipper wear causes tests to be costly; current slippers are single-use and discarded after each run (Hooser). Transfer of worn slipper material onto the track also requires post-test cleanup of the 11-mile-long track. In addition, the compounding nature of wear over the duration of the test run negatively impacts test quality and accuracy (Yeo, Palazotto and Song). Wear along the lips of slippers may also reach a point where total breakage occurs mid-testing, causing the sled to derail from the track and triggering catastrophic failure (Hooser). As such, it is

important to characterize the nature of wear under test conditions and to develop an approach to mitigate wear-induced damage.

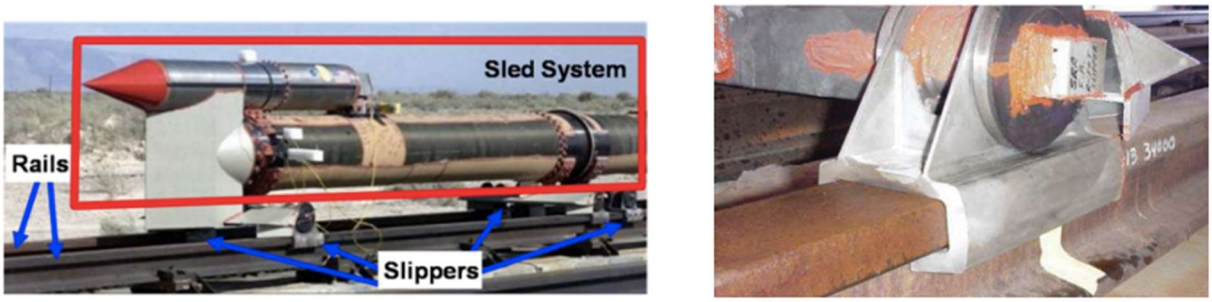

(a) Rocket Sled System (b) Slipper/Rail Interface

Figure 1.1 HHSTT configuration**.**

Currently, there are numerous experiments and models that evaluate aspects of wear experienced on HHSTT's slippers. However, there remains an incomplete understanding of the exact mechanics behind wear behavior. As such, attempts at improving slipper wear in the past have largely involved a "guess and test" approach (Hooser). To address this issue, this work uses Design of Experiments (DOE) to systematically identify and evaluate potential slipper attributes that improve wear-rates.

Ideally, a DOE would be conducted on the system in question itself, i.e., HHSTT. However, past endeavors have shown it is costly to conduct full-scale testing on slipper design alternatives. In addition, unfavorable responses in this environment could translate to catastrophic and potentially dangerous results. Instead, the Air Force Research Laboratory's (AFRL) high-speed pin-on-disc experiment attempts to simulate the velocity and contact force profiles of Vascomax®300 upon AISI 4340 on a smaller scale. This pin-on-disc rig is the only experiment that models these conditions in a controlled laboratory setting.

Although the scale of this rig is drastically decreased from that of the HHSTT, purchase and preparation of materials for use in experimentation is still costly and time consuming. In addition, there remains an enormous number of potential designs to consider. It is therefore

exceedingly important for AFRL to receive informed design recommendations before conducting acquisitions or live testing. This research identifies design aspects that mitigate wear by examining mathematical models of wear behavior on the pin-on-disc rig.

There are several models that attempt to describe wear behavior of a Vascomax®C300 specimen on AFRL's pin-on-disc rig. Boardman and Wing's models both use data from a 2019 run to analyze wear as solely a function of heat transfer (Boardman iv, Wing iv). Boardman's model uses a two-dimensional (2D) nonlinear heat transfer equation to predict material removal (iv), while Wing concludes that a one-dimensional (1D) approach with constant parameters generates a sufficient model (63-64). Of the solution methods tested by Wing, the one-dimensional transient finite element analysis (FEA) proves to provide accurate temperature profile predictions and be easily implementable in the computer simulation software ABAQUS (Wing 63-64). As such, this research uses the 1D transient FEA computer simulation of the pin-on-disc rig to conduct a DOE. This DOE screens for the most significant design factors, characterizes the wear response relative to these factors, and finds the factor levels for a more wear-resistant slipper design.

An additional aspect to the experimentation process is model validation. The FEA model on which the DOE is conducted is assessed for validity and robustness. The model is constructed using data from a single 2019 experimental run of the pin-on-disc rig. To determine whether the FEA model truly reflects overall behavior of the pin-on-disc experiment, additional runs are conducted on the rig. The response of the current model is then statistically compared against the data collected from the additional test runs to determine model accuracy.

1.2 Problem Statement

The goal of this research is to methodically determine ideal HHSTT slipper design specifications using a DOE approach. The DOE is conducted on the 1D transient FEA model of AFRL's pin-on-disc experiment. As this model represents wear using solely heat transfer, the resulting recommendations optimize wear according to a heat transfer perspective. This research concurrently assesses the FEA model of the pin-on-disc experiment for robustness and validity. The results provided by this research allow for informed decisions for expanded live testing on AFRL's pin-on-disc rig. Tested materials that show positive results on the rig may then move forward to testing on the HHSTT.

II. Literature Review

2.1 Design of Experiments

2.1.1 Fundamental Principles

One of the fundamental motivations behind experimentation is the need to improve a system in which developers do not have complete process knowledge. To date, no mechanistic model can completely capture the behaviors of HHSTT slippers, so it is not practical to make design improvements based on principles alone. A number of ill-fated slipper design updates have performed contrary to the expected behavior dictated by process knowledge (Hooser). Experimentation allows for the development of an empirical model, which is based on observational data rather than pure scientific or engineering principles. This empirical model can be informative in many ways, including identification of significant factors and providing an optimal design.

The major preliminary step to experimental design is identification of response variables and factors. Response variables are measurable outputs of interest. For this DOE, there is a single response of interest: slipper wear. Factors are the inputs that drive the behavior of the system response. It is important to distinguish between controllable and uncontrollable factors, as controllable factors are treated as design factors while uncontrollable factors may be addressed with mitigating tactics such as randomization and blocking. For each controllable factor, it is necessary to determine the range of experimentation. The specific values that are tested and identified within a factor's range are referred to as factor levels.

Another important consideration in modeling design factors is the specification of the model. This means considering whether the model is linear or if there is some curvature, such as interaction between different factors or quadratic factor terms. Process knowledge, or knowledge

of the system's mechanistic behavior, is useful to estimate the correct model specification. In the case of this research, there are mechanistic models that demonstrate nonlinear behavior in high-speed sliding wear. Therefore, curvature terms are considered in the model specification.

After preliminary design analysis is complete, experimental runs are designed. The process of conducting runs is sequential in nature; information gleaned from initial runs is used to determine the nature of further experimentation, which provides further information for proceeding steps, and so on.

2.1.2 Screening, Characterization, and Optimization Designs

The preliminary step to experimental design is screening to determine factors that are significant contributors to the response. This is done by estimating the magnitude and direction of factor effects, or how much the response variable changes when each factor is changed (Montgomery 8). If the coefficient on the factor effect has a non-zero magnitude (determined as an associated p-value of less than 0.05), the factor is deemed significant. Determining significant factors through screening is useful when there are many, i.e., four or more factors or when there is low understanding of the process (Muhamed). Usually, screening investigates only factor main effects and two-factor interaction effects.

The next level of experimentation is characterization. This design type considers a handful of potentially significant factors' main effects as well as curvature. The curvature is usually characterized by two-factor interactions and quadratic effects. After characterization, the next level in experimentation is optimization designs, which include response surface methodology designs and complex fits, such as Box-Behnken Designs and Flexible Fast Filling Designs.

2.1.3 Employed Experimental Design Types

There are several types of experimental designs that can be used to generate an empirical model. These include the Box-Behnken Design (BBD) and Space-Filling Designs (SFD). The BBD is a design made up of axial points along the edges of the design space and center points, as shown in **Figure 2.1**. These points are used to capture the curvature of a second-order model. A notable aspect of BBDs is that they exclude the extreme points on the corners of the design space, which is useful in instances where these extremes are infeasible. BBDs require at least three factors and contain three levels on each factor. Because BBDs are spherical, at least 3 to 5 center point runs are used to estimate pure error and test lack of fit.

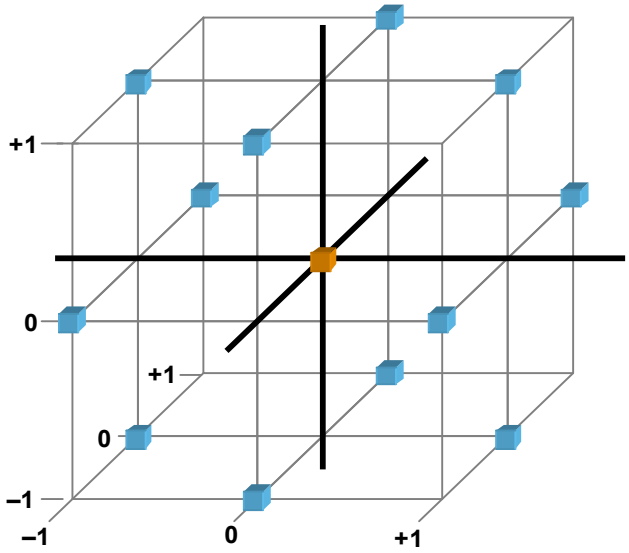

Figure 2.1. BBD points create a spherical design region, made up of axial points (blue) and center points (orange).

For experiments that employ computer models, space-filling designs are often appropriate. SFDs seek to cover as much of the design space in a near even or uniform fashion. These designs usually do not include replication, so they are useful for deterministic experimentation like computer simulations, where there is no run-to-run variability. Like BBDs, these designs can capture nonlinear behavior across different regions of the design space (Montgomery 536). This research uses SFDs to fit a second-order polynomial model as given in

equation (1) in **Section 2.1.4**. SFDs are also used to generate interpolated models as determined by the Gaussian process in **Section 2.1.6**.

One type of SFD is the fast flexible filling design (FFFD), which supports placing design points in a non-rectangular region (Jones and Lekvietz 5). An example using this type of design is shown in **Figure 2.2**. The FFFD is useful in cases where there are certain regions of infeasibility across the factor space. For this research, this occurs when certain material property combinations are infeasible across some factor range combinations. A common criterion used to generate FFFDs is the maximum projection (MaxPro) criterion. MaxPro maximizes the product of the distances between potential design points in a way that involves all factors. This supports the goal of providing good space-filling properties on projections of factors (Jones and Lekvietz 5)

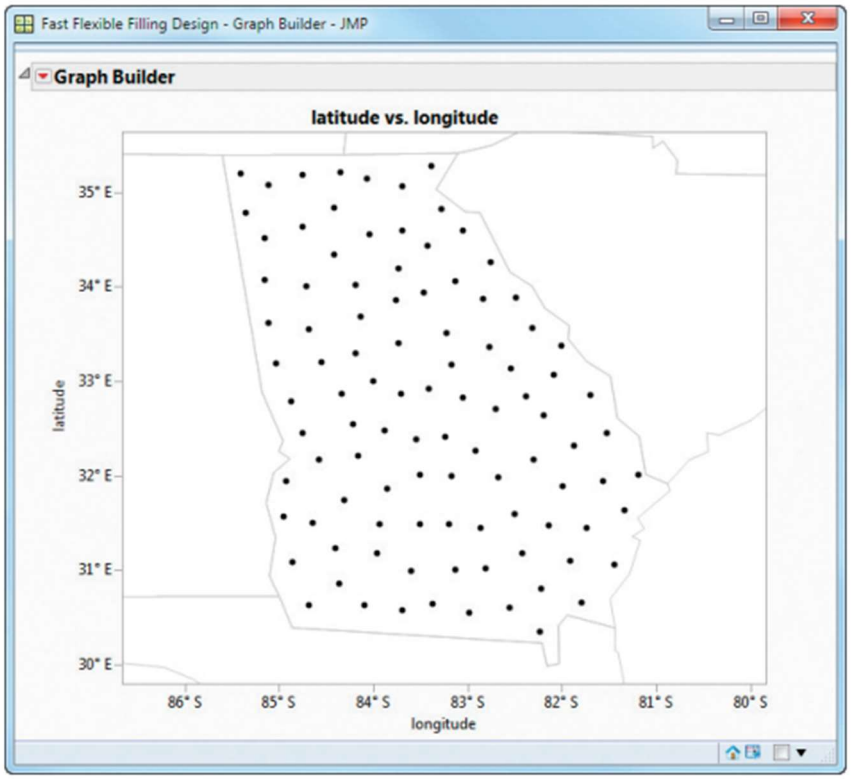

Figure 2.2. Fast flexible filling design created in JMP, with non-rectangular design space across factors latitude and longitude (Jones and Lekvietz 5).

2.1.4 Response Surface Methodology Principles

Response surface methodology (RSM) is a collection of statistical and mathematical techniques used for developing, improving, and optimizing processes (Montgomery 490). For this research, RSM is used to determine the region in the factor space that yields the optimal response. An example of RSM used in a similar application is shown in **Figure 2.3**, where the problem is to maximize a response of yield. A characterization experiment has identified factors of interest to be time and temperature. The lines of constant yield are connected to form response contours, and the entire surface is referred to as the response surface (Montgomery 9).

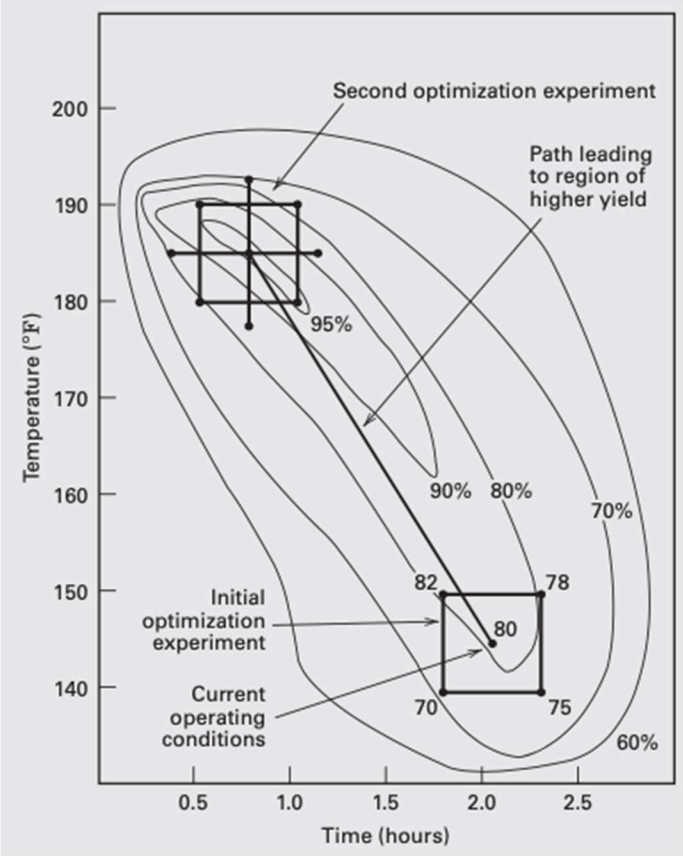

Figure 2.3. Response surface of yield as a function of factors time and temperature (Montgomery 9).

RSM is usually performed as a sequential methodology. Although there are multiple RSM techniques that can influence the exact sequence of steps, the initial phase generally begins with identifying response variables and potentially significant factors. In this research, the next step involves implementing a RSM design that can estimate a second-order model in the form of:

$$y = \beta_0 + \sum_{i=1}^{k} \beta_i x_i + \sum_{i=1}^{k} \beta_{ii} x_i^2 + \sum_{i<j} \sum \beta_{ij} x_i x_j + \epsilon \tag{1}$$

where y is the response, x represents the factor effects from a total of k factors, β represents the coefficients (including the intercept β_0), and ϵ represents the error term. This model captures curvature in the system behavior, and is used to identify the response optimum as well as associated factor settings (Montgomery 490).

This second-order model estimates the optimal set of operating conditions for the *x*'s and characterizes the nature of the response surface. Stationary points estimate maximums, minimums, and saddle points on the surface. These can be found by generating contour plots using computer software when fewer factors are involved. Eigenanalysis characterizes the shape of the generated response surface, and optimization locates stationary points to a reasonable degree of precision (Montgomery 491).

2.1.5 Analyzing the Response Surface Design and Model

A good experimental design has features that contribute to obtaining a reliable model. These features include a minimal prediction variance. Good designs also avoid factors that strongly correlate with each other, as this could lead to issues with aliased factor effects. This is when the effects of certain factors or factor combinations are confounded with each other, making it difficult to identify the true behavior of the system. Correlations between effects can

be examined through a correlation map, in which light colors represent little to no correlation and dark represents significant or 100% correlation.

The resulting second-order model of a designed experiment is analyzed according to numerous criteria. Generally, the first step of analysis is to determine significant factors that contribute to the model. This research uses backwards stepwise regression (starting from the highest p-value and working down), to determine these factors. The significance level used is $\alpha = 0.05$. This level is used as a baseline rather than a hard rule, as it is important to maintain model hierarchy. This is where main effects that may have $\alpha > 0.05$ are kept in the model if there are interaction terms that include said effect. Effects that are very close to the α level may also be kept if they significantly improve model performance.

Performance is determined by model fit, which can be measured in R^2 and R^2_{adj}. Both these metrics measure how well the data fits the model by measuring the proportion of total variation explained by the model effects. R^2_{adj} also considers the number of predictors in the model. This makes R^2_{adj} a generally more reliable metric in evaluating DOEs, because simply adding more factors into the model can inflate R^2. R^2 values can range from 0 to 1, with 0 meaning no correlation and 1 meaning perfect fit. R^2_{adj} values are generally close to, but lower than R^2 for a given model.

Analysis of variance (ANOVA) is used to evaluate model significance. A significant model results in a p-value of lower than $\alpha = 0.05$. The null hypothesis of this test is that none of the identified factors have an effect on the response. A small p-value indicates rejection of this hypothesis, meaning that at least one of the identified factors is a predictor for the response.

Models must also be evaluated for adequacy. This is done through examining the residuals, or error, to determine if the assumptions associated with the error term hold. One

important assumption is that residuals are of approximately constant variance. This can be evaluated by examining a plot of studentized residuals vs predicted values. A plot with points that are near-uniformly scattered across the plot indicates reasonable satisfaction of the constant variance assumption. Conversely, a plot with notable structure such as curving or funneling is unsatisfactory. Another assumption that is checked in evaluation of model adequacy is that residuals are approximately normally distributed. This can be examined through a normal probability plot, which plots residuals vs normal quantiles. This plot should closely follow a 45-degree line; severe deviations from this line indicate violation of the normality assumption, and the model should be reevaluated.

Severe deviations in either the studentized residuals plot or normal quantile plot may indicate outliers in the data. This can be formally evaluated using the Cook's Distance statistic, or Cook's D. Cook's D for the i^{th} observation removes that observation from consideration in the model and calculates how much the prediction changes with that observation removed. Cook's D values greater than 1 is usually evidence of an outlier.

Another common metric for evaluating models is the Variance Inflation Factors (VIFs), which checks for multicollinearity among the model effects. Ideally, the effects are not multicollinear, and they are independent from one another. VIF values close to 1 indicate satisfactory levels of independence, while values of 10 or more indicate multicollinearity.

The response of the second-order model can be analyzed to determine the estimated optimal response and its associated factor settings. A factor profiler, shown in **Figure 2.4**, is used to determine these values. The desirability of the response can be set to maximum, minimum, or a specific value. The profiler is used to identify the factor settings that result in the most desirable response. The factor profiler also reports the predicted value of this response and the

associated 95% confidence interval. Another way to examine the response is through a surface profiler, which gives a 3D visualization of the second-order model's response surface. This surface allows an experimenter to easily identify minima and maxima as well as the associated factor levels. Similarly, a contour profiler lays the response surface on a 2D contour map, with factors as the axes.

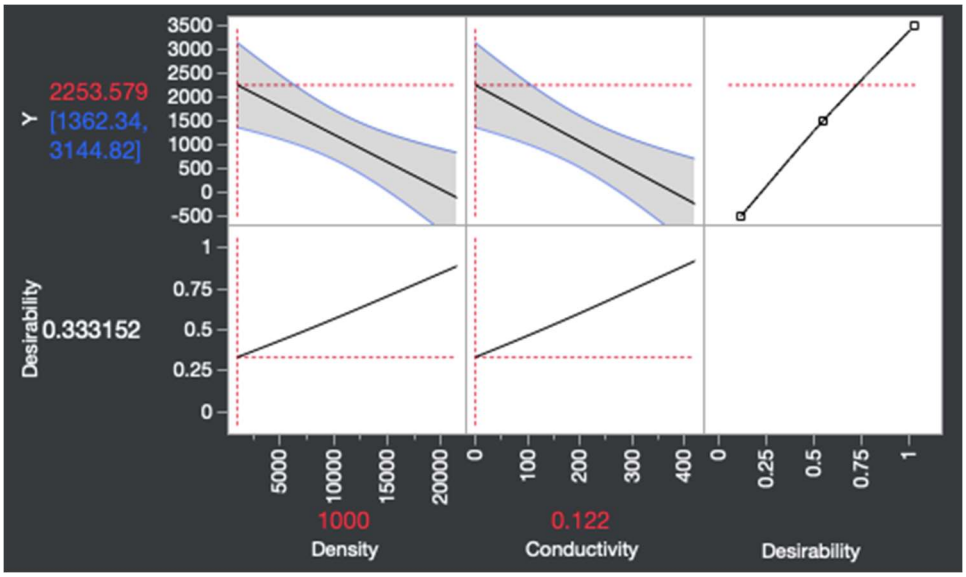

Figure 2.4. Factor profiler with factor settings on the bottom and response (Y) prediction on the left.

2.1.6 Gaussian Process

One alternative to using a response surface method to analyze experimental designs is the Gaussian process, also known as the Kriging method. While RSM is usually centered on a second-order model as given in equation (1), the Gaussian process uses interpolation to estimate a model that does not have to take on this specific form. This means that higher order curvature can be estimated. However, this also means that the generated model is usually more complex.

The Gaussian process considers the distance and degree of variation between known data points to estimate the value and variance at unknown points. Known points are weighted depending how close they are to the unknown point, which results in optimal and unbiased estimates

(Worley). This process is suitable for deterministic simulation modeling, where there is no pure error (i.e., there are no repeated points necessary). It is ideally applied to a space-filling design, because the near-evenly applied design points bound model bias (Worley). One unique issue with the Gaussian process model is that because it interpolates, it cannot be used to extrapolate outside the design region. This may or may not be a drawback depending on whether the problem seeks information outside the specified design region.

The Gaussian correlation structure uses the product exponential correlation function with a power of two as the estimated model. This model assumes that the response is normally distributed with mean μ and covariance matrix $\sigma^2\mathbf{R}$, where σ^2 is the variance of the model parameters. The elements of the **R** matrix for continuous factors are defined as follows:

$$r_{ij} = exp\left(-\sum_{k=1}^{K} \theta_k \left(x_{ij} - x_{jk}\right)^2\right) \tag{2}$$

where *K* is the number of continuous factors or predictors, θ_k is the theta parameter for the k^{th} predictor, x_{ik} is the value of the k^{th} predictor for subject *i,* and x_{jk} is the value of the k^{th} predictor for subject *j* ("Gaussian Process"). The parameters μ, σ^2, and θ_k describe the estimated model, and are fitted using the method of maximum likelihood.

2.1.7 Analyzing the Gaussian Process Model

Like with a polynomial model, a Gaussian process model is evaluated based on the fit. Different model specifications can result in better or worse fits, as determined by metrics such as an actual vs predicted plot and the log likelihood. An approximate 45-degree line is considered ideal for an actual vs predicted plot. For log likelihood, a higher value indicates a model is a better fit for the data. This means that when comparing models using $-2loglikelihood$, a less negative number is a better fit.

The main specification choice for a Gaussian process model is whether to include estimation of the nugget parameter. The nugget is a ridge parameter that factors into the maximum likelihood estimation procedure. It is useful if the response has a high amount of noise, and it is desirable to smooth over the noise instead of perfectly interpolating ("Gaussian Process").

The Gaussian process model provides information in terms of total sensitivity, main effects, and interaction effects. The sensitivity is the sum of the main effect and interaction effects for each factor. It is a measure of the amount of influence a factor and all its two-way interactions have on the response variable. The main effect of each factor is the ratio of variation due to that factor alone and the total variation in the model. Similarly, interaction effects measure the proportion of variation due to each two-way interaction.

As with a polynomial model, the response of a Gaussian process model can be investigated using factor, surface, and contour profilers. The impact of each main effect on the response can also be visualized using marginal model plots, as shown in **Figure 2.5**. For each plot, all main effects except one are integrated with a uniform distribution over the factor ranges. The marginal prediction of the response for the remaining factor of interest is drawn in blue. The data points of the observed response values are included to show how well the marginal model fits the data ("Gaussian Process"). The behavior of the marginal model line indicates the effect of that factor on the response. Marginal model plots can also very flat, indicating that the factor has little to no leverage on the response.

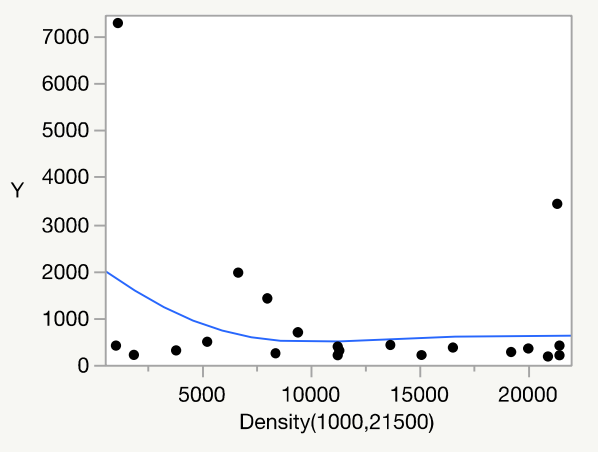

Figure 2.5. Marginal model plot generated from a Gaussian process model. The response is Y and the investigated factor is density.

2.2 Wear Models of the Pin-on-Disc Experiment

The most recent studies regarding HHSTT slipper wear-rates come from AFRL's 2019 high-speed pin-on-disc experiment. This experiment provides a simplified representation of the true force and velocity conditions that slippers experience while sliding along the HHSTT. The test rig for this experiment (**Figure 2.6**) consists of a drive stand mounted to a 12-inch diameter disc made of the track material, AISI 4340 steel (Wing 4). This disc spins against a pin, which is composed of material from a discarded test track slipper made of Vascomax®C300 maraging steel. The motor-actuated pin holder pushes the pin against the disc to maintain near-constant force as the pin wears down over the course of the experiment. The disc is capable of spinning at speeds up to 240 m/s (Wing 4); while this is a small fraction of the speeds experienced on the test track of over 2000 m/s, this simplified experiment usefully captures various aspects of wear behavior, including micromechanical wear and heat transfer.

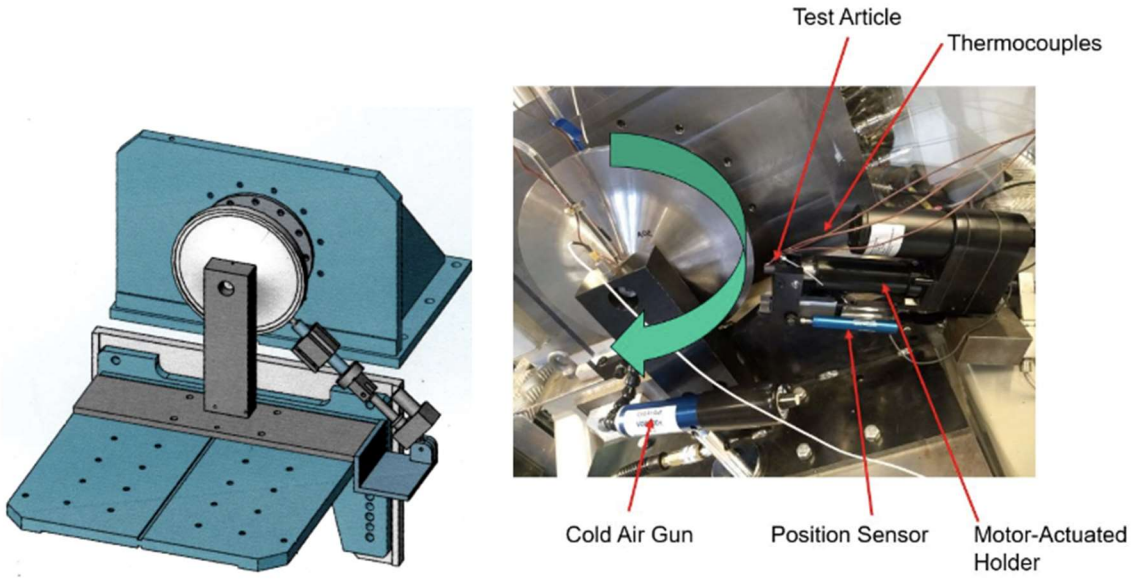

(a) Rig Design (b) Test Rig

Figure 2.6. 2019 Pin-on-disc experiment concept design (a) and rig parts (b) (Wing 4).

2.2.1 Micromechanical Models

Micromechanical analysis of pin-on-disc wear is conducted through observation of the worn pin specimens. As shown in **Figure 2.7**, the face of worn pins display a "mushrooming" effect that is indication of plasticity, or permanent deformation of the material. This deformation is due to the stress, or force per area, applied to the material. In metals such as Vascomax, the presence of plasticity indicates internal sliding along the planes of the material's molecular structure. Plasticity in the metal additionally indicates that the material reaches high temperatures over the course of a run, which make the material more susceptible to permanent deformation.

Liu's microstructural analysis of worn pin-on-disc specimens finds that the region closest to the worn face of the pin are made up of coarse grains compared to the rest of the material (3). Liu postulates that this is an indication of recrystallization due to high plastic shear strain and high temperatures (11). Shear strain is deformation as a result of shear force applied to the material. In this deformed region, worn material accumulates in the direction of the velocity, as shown in **Figure 2.7**. The presence of plasticity in these worn specimens in indication of internal

plastic shear, which can generate a local temperature increase given a high enough stress. This heat is in addition to the heat transfer due to frictional heating through the face of the pin.

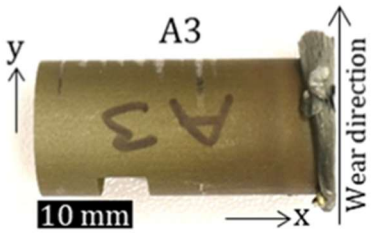

Figure 2.7.

Figure 2.7. A worn Vascomax®C300 pin specimen (Liu 9).

The fine grain type present in this region manifests at temperatures around 70% of a material's melting point, which for Vascomax®C300 T_{melt} = 1685.95 K. The estimated temperature reached in this region is therefore 70% of 1685.95 K = 1180 K. At this temperature, the material becomes austenitic, but when cooled becomes martensitic again. The final microstructure of the specimen is primarily martensitic (Liu 17).

The next region in the pin has reduced hardness but no significant grain structure change, which indicates the temperature is high enough to coarsen the strengthening precipitates, but not high enough to cause significant grain growth. This indicates temperatures in excess of 900K, but below 1180K (Liu 17). In this region, the plastic shear pattern is in the direction of wear, as shown in **Figure 2.8**. **Figure 2.9** shows the estimated temperatures reached throughout regions of the pin.

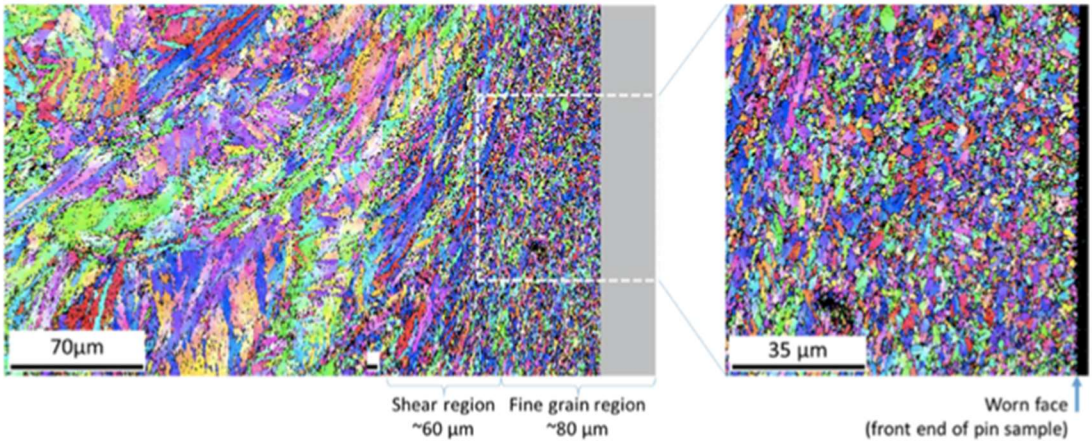

Figure 2.8. Microstructural grain patterns of experimental specimen (Liu 15).

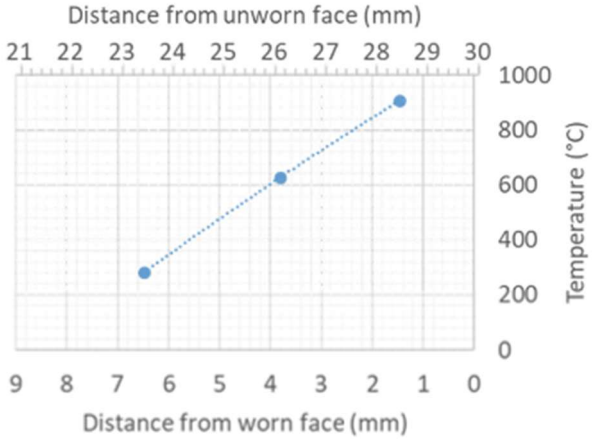

Figure 2.9. Temperature estimates for regions of the pin (Liu 18).

2.2.2 Heat Transfer Models

While micromechanical behavior is used to characterize the wear response, direct experimentation in this research is performed with Wing's finite element analysis (FEA) heat transfer model. Where Liu's work observes wear through a micromechanical lens, Boardman and Wing's models examine pin-on-disc wear based solely on heat transfer (Boardman iv), (Liu 3), (Wing iv). Heat transfer is thermal energy in transit due to a spatial temperature difference. Heat energy transfer occurs in the direction from high to low temperature (Bergman, Lavine and Incropera 3).

Experimental thermal data, captured through thermocouples bored into the specimen, is a basis for these heat transfer models. The three thermocouples (T_1, T_2, T_3) are bored into the specimen at 0.125, 0.250, and 0.375 inches from the pin face at 30-degree angles, as shown in **Figure 2.10**. The thermocouples used in the pin-on-disc test are type J, which are rated for temperatures up to 1030 K. The error on these thermocouples is ± 0.75%. The heat transfer data that results from the thermocouple measurements is shown in **Figure 2.11**.

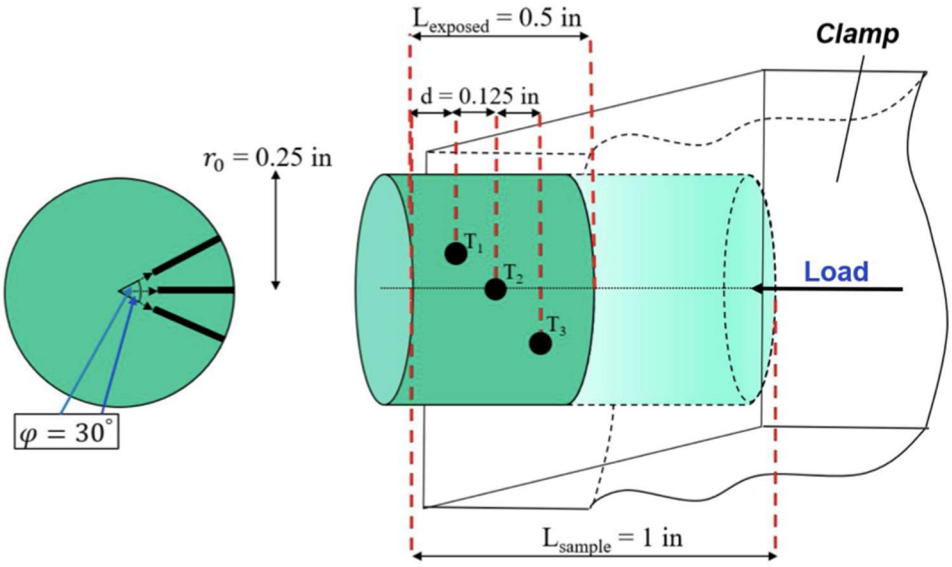

Figure 2.10. Thermocouple placement in pin to measure heat transfer, as represented by T1, T2, and T3 (Wing 4).

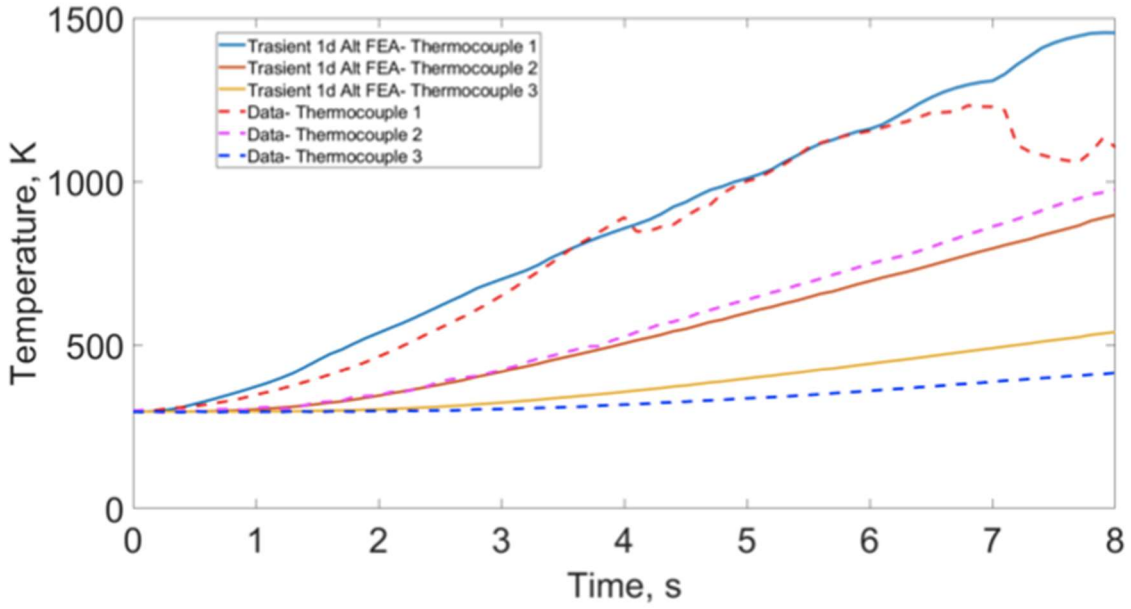

Figure 2.11. Experimental temperature data compared to Wing's 1D transient FEA model estimations (Wing 32).

Boardman uses a two-dimensional nonlinear model to predict heat transfer on the pin-on-disc experiment. Wing builds off this work to conclude that a one-dimensional approach generates a sufficient model. In particular, Wing's 1D FEA with constant parameters and a transient solution method generates a representative temperature profile of the empirical data. Finite element analysis is a method for numerical solution of field problems such as the distribution of temperature in a specimen. Individual finite elements are represented as small pieces of a larger structure. The temperature through each element is assumed to have simple variation defined by a shape function (Wing 16). FEA therefore provides the approximated temperature variation throughout a body where the distribution is continuous across the element connections, or nodes. A particular arrangement of nodes that make up a shape is called the mesh, and can be represented by a system of algebraic equations where the nodal quantities represent the temperature. Solving these equations approximates the temperature distribution (Wing 16).

Wing's FEA model, generated and executed in ABAQUS simulation software, is able to quickly compute temperatures through the specimen using this method. This FEA model is also suitable for experimentation because various material properties, i.e., design factors, can be toggled to give unique temperature profile outputs. Given these considerations, this research uses the 1D FEA model to conduct experimental design.

The surface heat flux equation used by the FEA to describe heat transfer through the pin is given by equation (3) (Wing 24). This equation for heat flux q in units Watts/meter^2 (W/m^2) is applied to each sequential material removal at the face of the pin:

$$q(t) = \frac{\beta(t)\mu(t)F(t)v(t)}{A(t)} = 5.950 \cdot 10^6 \ \frac{W}{m^2} \tag{3}$$

where β is the partition function, μ is the coefficient of friction, F is the applied force, v is the velocity of the pin relative to the rig, and A is the area of the pin face. The flux parameters are treated as constants to describe the pin-on-disc test environment, with values given in **Table 2.1**. Material removals are given in **Table 2.2**.

Table 2.1. FEA flux parameters (Wing 24).

Parameter	Value
$\beta(t)$	0.12
$\mu(t)$	0.20
$F(t)$	656.76 N
$v(t)$	47.83 m/s
$A(t)$	0.0001276 m^2

Table 2.2. FEA material removals (Wing 23).

Step	Total material displacement (m)	Total time (s)
Initial	0.00	0
1	0.00	0-1
2	0.00005	1-2
3	0.000125	2-3
4	0.00035	3-4

5	0.0007	4-5
6	0.0011	5-6
7	0.0015	6-7
8	0.0020	7-8
9	0.0022	8-9

The 1D FEA generates a temperature profile based on experimental material removal data, given in **Figure 2.12**. This wear data is taken in timesteps of 1 second, so the model is partitioned by these sequential removals. **Figure 2.13** shows the model in ABAQUS, which is built off of a cross-sectional representation of the pin. Finite elements are implemented in the form of a nodal mesh (**Figure 2.14**) so that temperatures can propagate through the model according to constant parameter values for flux and material properties. Temperature profiles are then generated from the nodes at each of the three thermocouples. In summary, this model estimates temperatures through the specimen over the course of the wearing event.

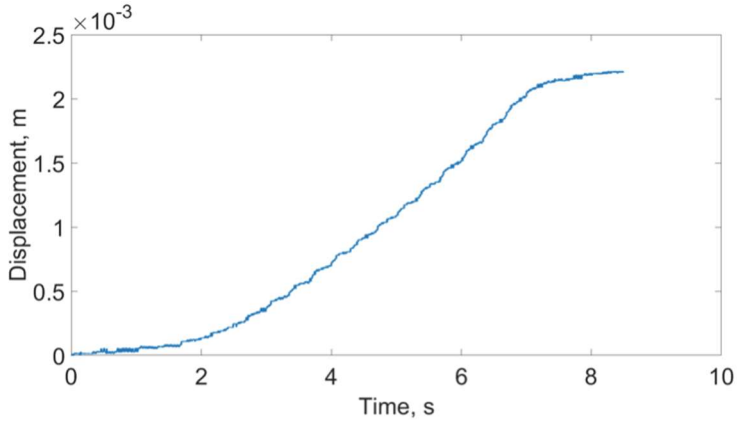

Figure 2.12. Material removal data from 2019 experimental run.

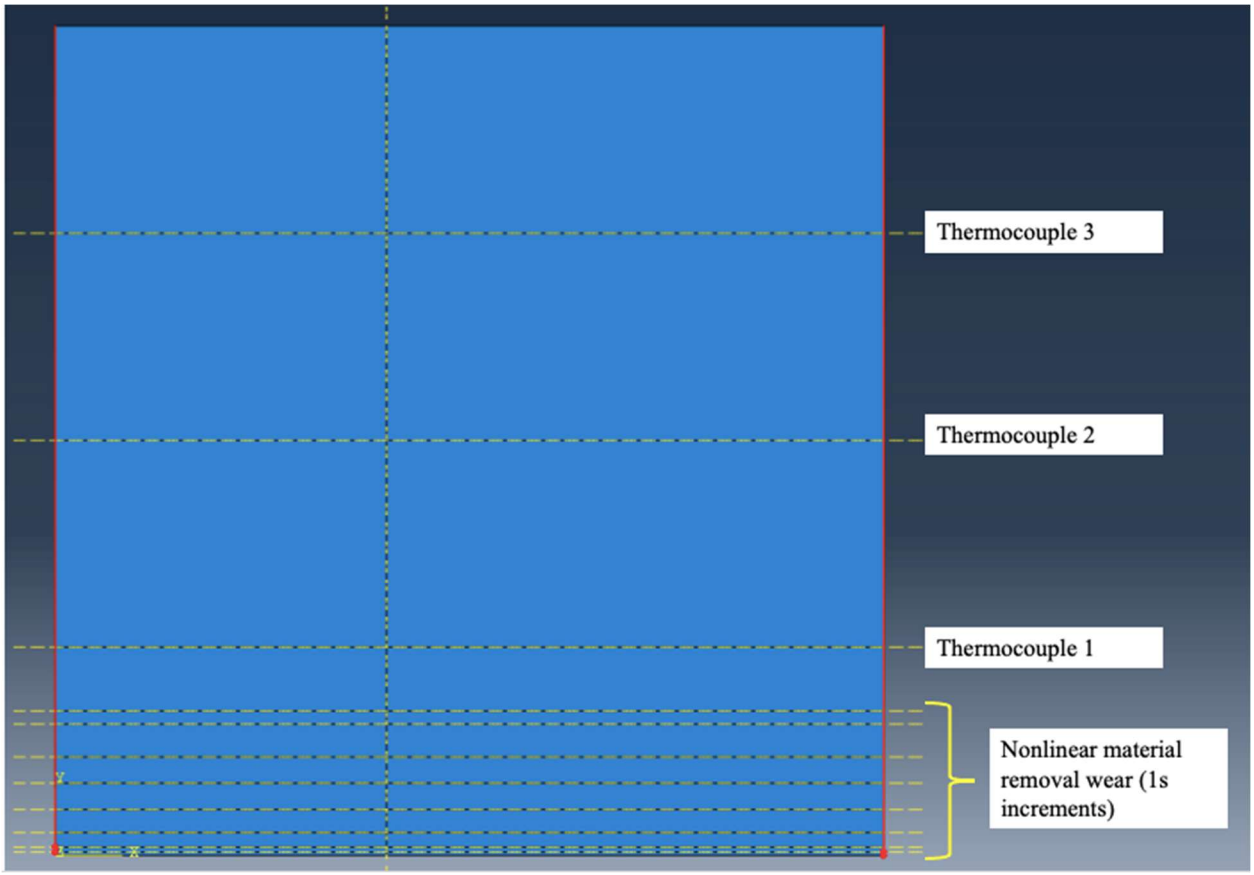

Figure 2.13. Wear representation in FEA model through material removals.

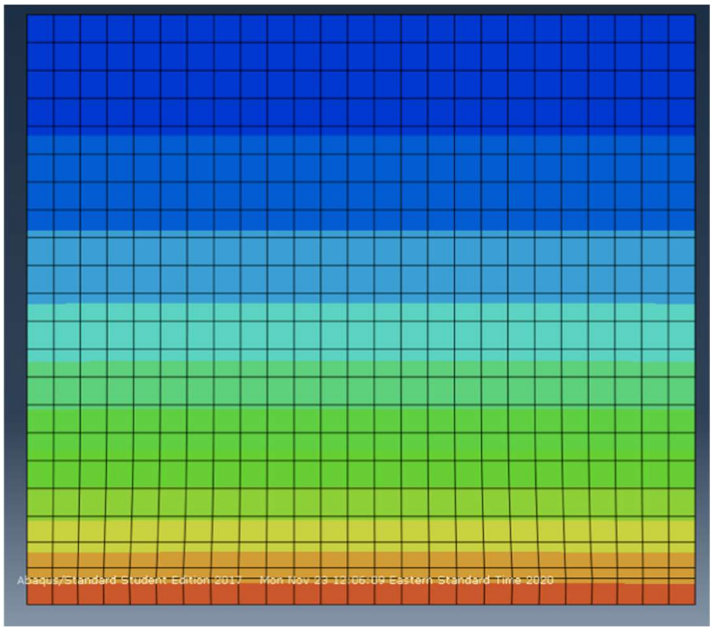

Figure 2.14. Temperature flowing through finite elements, represented by nodal mesh in ABAQUS.

2.3 Characterizing Slipper Wear

The most widely accepted definition of wear is "the loss of material from a surface, transfer of material from one surface to another, or movement of material within a single surface" (Hutchings 1). Given this general description, Bayer elaborates that wear is a system rather than a material property (2). Wear can be caused by various mechanisms and combinations of mechanisms, depending on the tribosystem context. "Wear behavior is frequently nonlinear. Transitions can occur in wear behavior as a function of a wide variety of parameters" (Bayer 2). These parameters may include velocity, temperature, friction, and material characteristics. From these varying parameters also arise a variety of wear responses, such as material removal, surface deformations, internal deformations, and melt. One of the first steps of this DOE characterizes high-speed slipper wear by identifying an appropriate metric for the wear response and determining controllable design parameters which dictate the response.

2.3.1 Wear Response

The response for this experimental design is slipper wear performance. As such, this research seeks to optimize the variable chosen to represent this response. To determine an appropriate metric for wear performance, it is important to first understand the nature of wear behavior. Lim and Ashby's comprehensive wear map of steel, shown in **Figure 2.15**, characterizes different wear responses based on input parameters most closely associated with the wear process: normalized force ($\tilde{F}$) and normalized velocity ($\tilde{v}$). Their work also analyzes the impact of thermal effects across these different regions. The majority of the data used to build this map is from a series of 1980s dry sliding, pin-on-disc experimental tests (Lim and Ashby).

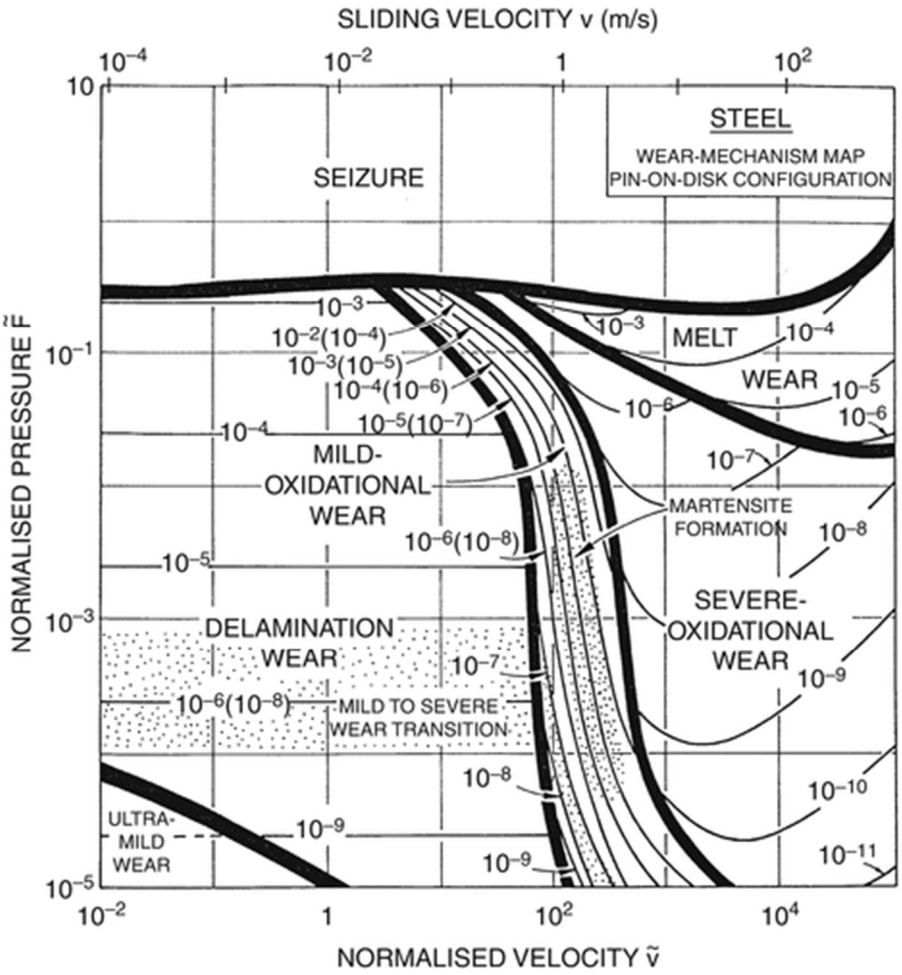

Figure 2.15. Lim and Ashby wear map of steel.

The map in **Figure 2.15** shows regions of wear types across a factor space of $[\tilde{F}, \tilde{v}]$. The lines on the map represent possible areas of transition from one form of wear to another; they are not precise and are only used to express general behaviors (Boardman 19), (Lim and Ashby). These wear types are described (in approximate order from low to high regions across $[\tilde{F}, \tilde{v}]$ space): ultra-mild wear, delamination wear, mild-oxidational wear, severe-oxidational wear, and melt wear. Ultra-mild wear occurs while the oxide layer formed between the materials remains intact (Boardman 19). Delamination wear occurs when surface cracks cause shearing the material in thin sheets. Mild-oxidational wear is described as the splitting off of the brittle oxidation layer (Lim and Ashby). The wear in this region may also be influenced by a phase

change to increased material hardness, which equates to a sudden decrease of the wear rate. Other than this factor, thermal effects have little impact in the regions of ultra-mild, delamination, and mild-oxidational wear (Hutchings 17).

Severe-oxidational wear occurs when the surface temperature is high but not yet at melt, and material continues to be removed from the oxide layer but not yet the metal. Wear is more continuous in this regime, and may be due to abrasion or melting of the oxide. Finally, melt wear of the metal occurs when temperatures are so high that thermal conduction becomes ineffective at removing heat from the surface. This melt may cause a layer of lubrication that decreases the coefficient of friction values, but is still characterized by higher wear rates due to the ease with which the molten material is removed. Because temperatures are so high, oxidation wear is likely also present (Boardman 19), (Lim and Ashby). Both severe-oxidational and melt wear are greatly impacted by thermal effects, and these regions are of particular concern when it comes to high wear-rates.

Another predominant wear characteristic comes from mechanical behaviors of the sled sliding along the track. In investigation of HHSTT slipper wear, Yeo finds that when slippers impact a roughness on the track, deformation occurs at the surface of the slipper (Yeo, Palazotto and Song). These areas of roughness, also known as asperities, are on the scale of a several micrometers. One type of deformation that can occur on the slipper surface plowing, which is a continuous scratch pattern present in sled velocities of around 20 m/s (Yeo, Palazotto and Song). Gouging is another type of deformity that presents as a teardrop-shaped groove in the surface of the slipper at higher velocities, around 200 m/s. Gouging and plowing damage patterns observed after a 2008 HHSTT test run are shown in **Figure 2.16**.

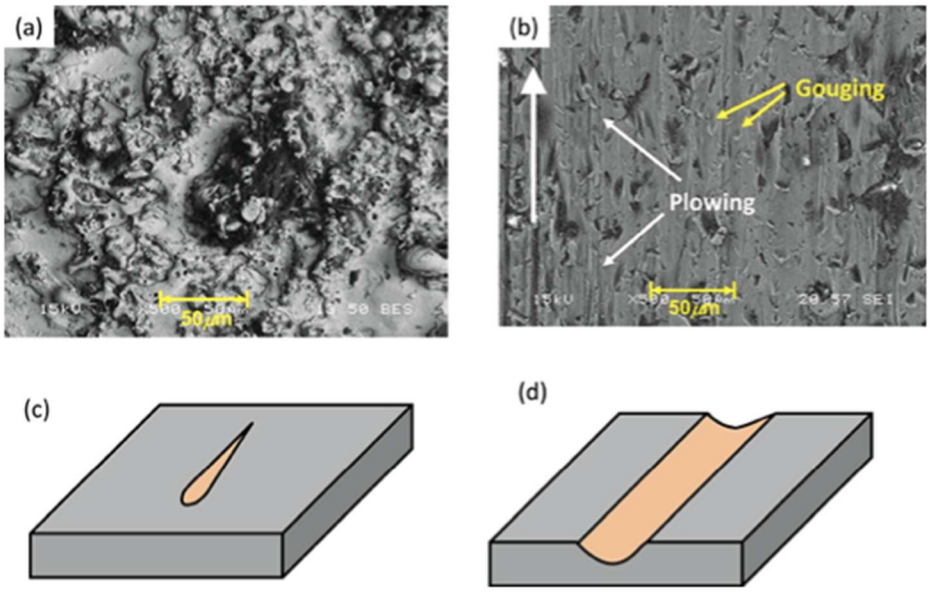

Figure 2.16. Scanning electron microscope (SEM) images of the slipper surface (a) before and (b) after the 2008 test mission in HHSTT, as well as (c) and plowing (d) schematics (Yeo, Palazotto, and Song).

In Sandia National Laboratory's 1968 rocket sled tests, Gerstle et. al. find that high-speed asperity impacts can cause shear. This is when the impacted material experiences internal micromechanical sliding. These findings are consistent with the micromechanical analysis of worn pin-on-disc specimens of **Section 2.2.1**. The results of both tests suggest that high-speed wear of metal slipper material is associated with stress-induced micromechanical sliding along internal surfaces.

In the case of the Sandia tests, Gerstle finds that when a high-temperature projectile (e.g., a slipper) impacts a target (e.g., a rail) with a severe combination of thermal energy and high velocity, layers of local temperature differentials occur. The stress of the impact causes internal mechanical deformation, which in turn causes additional heating of the material. The temperature differentials induced by this behavior are so high that the local rate of temperature change softens the material quicker than strain hardening can strengthen it. It then becomes an area of

local weakness in the material, which makes that area susceptible to catastrophic thermoplastic shear (Gerstle, Follansbee and Pearsall), (Szmerekovsky 10).

These shear bands are present in areas where the force of the slipper impacting an asperity causes a gouge. The bands are located below the surface of the gouge, and are characterized by microcracks known as shear fractures. These areas of shear are problematic, as they can induce additional heating of the material at that site. Higher temperatures make the material more susceptible to plasticity, or permanent deformation. This type of wear is additionally problematic as aggregation of cracks within the material can lead to catastrophic shattering of the slipper (Hooser).

2.3.2 Slipper Design Factors

In the current experimental design, factors are design attributes that potentially influence slipper wear performance. Controllable factors investigated in this research involve the material composition of the slipper. The current slippers are composed of Vascomax®C300 maraging alloy steel. "Maraging" refers to a type of steel that is fully hardened to a martensite structure and is strengthened by aging. "300" refers to this material's approximate yield strength of 300 kilopound per square inch. Maraging steel is unique in that it has both high strength and high ductility. Its high strength makes it suitable for bearing heavy loads, and high ductility gives it high damage tolerance (Liu 3). Despite these favorable characteristics, current Vascomax slippers experience documented issues with wear at the HHSTT.

Because this research uses a FEA computer model to conduct experimentation, design factors are material properties controllable within this model. These factors are mass density (ρ), thermal conductivity (λ), and specific heat (c_p). These properties can vary within a given material depending on temperature. For example, mass density is a function of a material's

coefficient of thermal expansion as well as temperature (T). Specific heat is likewise a function of temperature, with values for Vascomax given by **Table 2.3**. Despite this, Wing's baseline FEA approximates these properties as constant, with values given in **Table 2.4**.

Table 2.3. Temperature and specific heat for Vascomax®C300 (Wing 10).

Temperature (K)	**Specific Heat, c_p, (J/(kg·K))**
298	360
422	481
598	599
700	858

Table 2.4. Vascomax®C300 material properties used in baseline FEA model (Wing 10).

Property	**Value**	**Temperature**
Density, ρ	8000 kg/m^3	All
Conductivity, λ	30.807 W/(m·K)	All
Specific heat, c_p	857.98 J/(kg·K)	All

Mass density represents material mass per volume in kg/m^3. Density plays a role in various other material properties, such as specific stiffness and specific strength. These are measures of a material's ability to withstand deformation under load given its density. While specific stiffness is a measure of how much materials elastically deform, specific strength is a measure of permanent deformation. Density also factors into how heat flows through a specimen (Wing 13). As discussed, the distribution and flow rate of heat energy through a slipper has considerable impacts on wear.

Thermal conductivity is also an important factor in heat transfer through a material. Thermal conduction is the rate at which heat energy transfers from adjacent molecules, whether through two materials in contact or through the body of a material (Gregersen). An example of thermal conductivity at work is Szmerekovsky's findings in the CTH simulation of the HHSTT scenario: adding an epoxy coating to the slippers decreases temperatures by half over the course of 20 microseconds (Szmerekovsky). This is because epoxy has a much lower thermal

conductivity (~0.3 W/(m·K)) than maraging 300 steel (30.807 W/(m·K)). However, it is notable that while epoxy has a higher thermal resistance, it has a lower resistance to impact (Szmerekovsky).

Specific heat, measured in J/(kg·K), is the amount of heat energy per unit mass required to raise the temperature by a unit amount, in this case Kelvin. As such, materials with high specific heats are useful for temperature regulation. For example, the specific heat of water is at least double that of any metal. This means much more total energy is required to increase the temperature of water than metal ("Internal Energy"). In choosing factor ranges and levels for specific heat, the engineering feasibility of potential slipper materials must also be considered.

III. Methodology

3.1 Find Region of Interest

To begin experimentation for optimal slipper design, an appropriate response variable and process variables are identified. The response variable is a measurable metric that characterizes the output in question: wear. This metric is the variable to be optimized using experimentation to find the best settings. Examples of potential responses in the context of this problem may include material removal, slipper temperature, or other indicators of wear over the course of a test run.

Process variables are factors that affect the slipper wear response. There are both controllable and uncontrollable process variables, also known as factors. Controllable factors relating to design are referred to as design factors. Examples of design factors may include the slipper material's specific heat, conductivity, coefficient of friction, and density. They may also include aspects like size and structure. There are also controllable variables that are not considered design factors. These are called held-constant factors, and include aspects that are not intrinsic to slipper design such as sliding velocity, normal force due to load, and any other factors related to the test environment. While these aspects have an impact on the wear response, they are not aspects of design. In this research, all experiments are set to a constant force, velocity, and run time for purposes of comparison and repeatability.

Uncontrollable factors in this case involve aspects of the experiment that may impact the response, but are beyond control to the actors involved in experimentation. For physical experimentation, this can include natural variation in mechanical behavior or human-in-the-loop processes. For a simulation, this can include software issues or unknown modeling errors. For

example, simulations built for one material but extrapolated to other materials will impact the measured wear result.

Once all factors are identified, significant factors are identified through screening and/or characterization. Screening is used in the case of many (four or more) potential design factors. Characterization involves a pared down set of factors, and examines the approximate behavior of the experiment. This includes determination of interaction and/or quadratic effects. Once the experiment is characterized, experimentation is designed and conducted to determine the approximate region in the design space that yields the best possible response. In this case, it determines the factor levels which yield an optimal wearing result. This region in the design space is referred to as the region of interest, and it is used for materials identification and analysis.

It is important that a suitable design is constructed for this step, as the design points and resulting response surface should accurately depict wearing behavior. Information gleaned through this process may also be used for augmented or improved experimentation. These results should also be independently useful to informing physical slipper design and analysis.

There are several design considerations throughout this process. Firstly, this design is conducted using the 1D transient FEA model of the 2019 pin-on-disc experiment. As such, potential process variables are limited to design factors that may be controlled in the model. In addition, real-world material characteristics must be considered. That is, there are a limited number of materials, treatments, coatings, etc., that are produced and are available for use. In addition, certain materials have properties that are not characterized by the pin-on-disc experiment. For example, ceramics are excellent at withstanding certain types of wear, but they shatter upon impact of blunt force caused by bouncing at the HHSTT sled track. These

considerations, which are often found through SME knowledge and literature, must be considered throughout design and experimentation.

3.2 Conduct Materials Analysis

Once the region of interest is determined, materials with specifications in and/or around this space are identified. Ideal slipper materials are identified as those that perform at or near the optimum response, as determined by the specified model. These materials should also aim to meet goals not encompassed within the scope of the DOE problem. One of these goals is cost effectiveness. This is analyzed using a cost curve and identifying materials that lie on the cost efficiency frontier. Other goals may include availability of the material in large quantities, existing engineering and industrial applications, malleability, and the ability of the material to withstand significant load and impact.

3.3 Validate Existing Pin-on-Disc Model

This work utilizes the FEA model of the pin-on-disc experiment to design and conduct a DOE. It is therefore important to assess the validity and robustness of this model. The current FEA is based off of a single 2019 run on the pin-on-disc rig. As such, additional replicated runs are conducted at AFRL to generate more data on the true behavior of Vascomax wear. Once these runs are conducted, the FEA model is statistically assessed against the full set of data to determine if the temperature profiles generated by the FEA are truly representative of the wear behavior. This is done using outlier analysis and by comparing the model-generated profiles to both the estimated true mean.

IV. Experimental Design and Analysis

4.1 Initial Design and Analysis

The initial phase of this DOE characterizes the experiment. This phase includes determination of the response variable, the factor space, and which factors significantly influence the response. Main effects, interaction effects, and second order effects are tested for significance in a Box-Behnken Design. In this phase, an initial response surface is generated to estimate where ideal designs may be located within the factor space. Process knowledge is also gleaned from analyzing how different factor combinations impact the behavior of the FEA model output.

4.1.1 Response Variable Selection

For this DOE, the selected response variable is maximum temperature change, $\triangle T_{max}$. This response is generated from simulated runs on the 1D transient FEA model of the high-speed pin-on-disc experiment. $\triangle T_{max}$ is calculated as the maximum temperature change observed by any thermocouple over the duration of a run, or $T_{max} - T_0$. An example measurement of this response on the Vascomax temperature profile is shown in **Figure 4.1**.

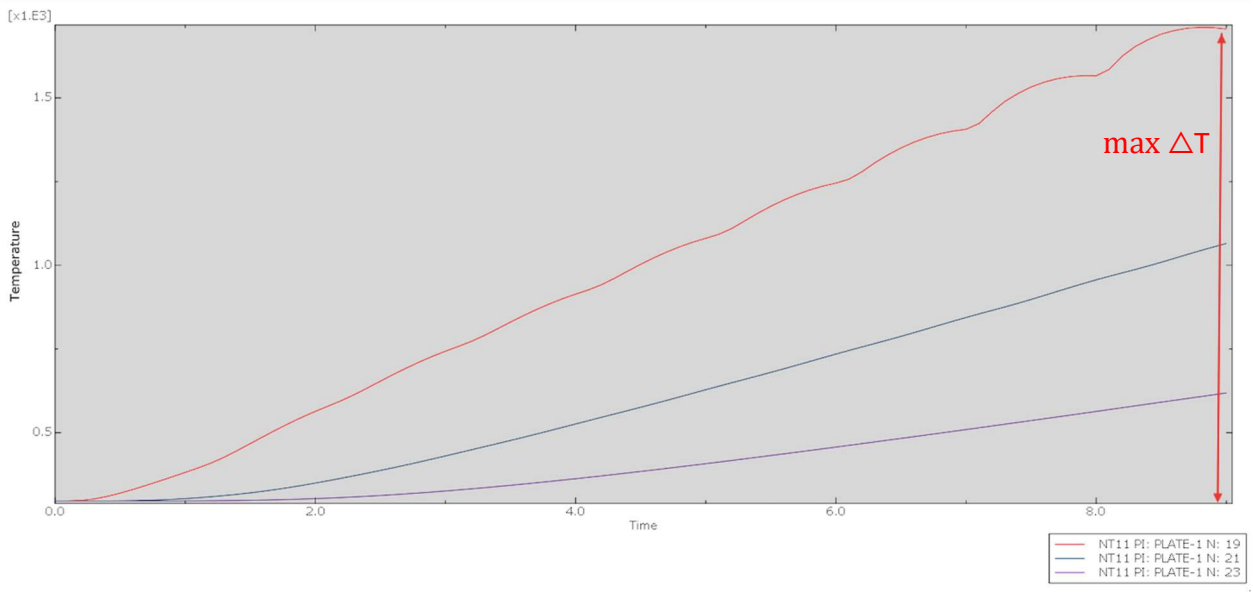

Figure 4.1. Example measurement of $\triangle T_{max}$ from the FEA temperature profile, baseline Vascomax®C300 specimen.

This response variable is chosen for several reasons. It is a metric that usefully captures the heat transfer information generated by the FEA. The FEA model gives numerous outputs which represent heat transfer through a material, such as heat flow visualization and temperature over time profiles. While all these graphics have value, $\triangle T_{max}$ is a single measurable output that can be inputted as data for the DOE.

There is also the mechanistic and most important reason $\triangle T_{max}$ is chosen as the response variable. There are broadly two known causes of specimen wear under the high-speed pin-on-disc environment: heat transfer and micromechanical wear. The FEA model simulates a fixed wearing event entirely due to heat transfer. However, it is known that micromechanical wear corresponds with additional problematic phenomenon such as plastic deformation, subsurface catastrophic thermoplastic shear, and microcracking. These events are not directly characterized by the FEA. However, model temperature profile results can indicate whether the wear event is predominated by heat transfer or by non-heat transfer induced wear such as mechanics.

It is best to *maximize* $\triangle T_{max}$ given by the FEA model, since a high $\triangle T_{max}$ signifies wear due predominantly to heat transfer. Conversely, an observation that undergoes the fixed wearing event with a $\triangle T_{max}$ significantly lower than melt cannot have worn due to heat transfer. Rather, the wearing event is likely due to mechanical wear, which is a more problematic mechanism in the context of HHSTT slippers. Thus, a high $\triangle T_{max}$is more ideal as the wear is predominated by heat transfer.

4.1.2 Determination of Factors, Ranges, and Levels

For slipper design, the factors of interest are the material specifications of a given specimen. Since this experiment is conducted using the FEA computer model, factors must also

be controllable as parameters within the model. They must also be reliably measurable across the entire region of operability. Ideally, specifications must apply to as many potential materials as possible. In other words, it is not good for a specification to only be measurable on certain types of materials. These considerations lead to the identification of three potential factors for design: mass density (ρ), thermal conductivity (λ), and specific heat (c_p).

Ranges for these factors are selected such that they span a wide enough testing region, but do not go outside the realm of feasible utility. Examples of properties outside the realm of feasible utility include specific heats above 3000 J/(kg·K), where materials become extremely flammable. Another example is materials with high densities above 22 kg/m^3, which display very brittle qualities. Therefore, range selection involves striking a balance between covering a broad enough region to test many possibilities and limiting the region to a tractable and useful scope. Limiting the range also improves the fidelity of the DOE model; a broader range generally requires more observations to capture potential curvature.

In conducting range research, there are three main categories of materials scoped. These are metals, engineering ceramics, and engineering plastics (Hooser). Each material type has an approximate range for the properties of density, conductivity, and specific heat. The range across all these categories can then be aggregated to construct a general range for each property. For example, ranges for mass density are observed across metals, ceramics, and plastics. Commonly used metals have a density range between 2,700 kg/m^3 (aluminum) and 21,500 kg/m^3 (platinum) ("Metal properties"). Engineering ceramics, also known as advanced ceramics, have a density range of 2,500 kg/m^3 (boron carbide) and 6,000 kg/m^3 (zirconia Y-TZP) ("Thermal Conductivity"). Engineering plastics, which include grades heat of heat-resistant plastics such as thermosets and thermoplastics, range between 1,000 kg/m^3 (acrylonitrile butadiene styrene

(ABS) and 2,200 kg/m^3 (Polytetrafluoroethylene/PTFE) ("Engineering plastics"). Therefore, the general range of mass density that should be tested is between 1,000 kg/m^3 and 21,400 kg/m^3. The full ranges for each material property are shown in **Table 4.1**.

Table 4.1. Factor ranges.

Material Property	**Ranges**			
	Metals	Ceramics	Plastics	Full Range
Mass Density (kg/m^3)	2,700 – 21,500 (aluminum, platinum)	2,500 – 6,000 (boron carbide, zirconia Y-TZP)	1,000 – 2,200 (ABS, PTFE)	1,000 – 21,500
Thermal Conductivity (W/(m·K))	15 – 420 (stainless steel 316L EN1.4404, silver)	1.5 – 150 (quartz, aluminum nitride)	0.122 – 0.41 (PEI, PBI)	0.122 – 420
Specific Heat (J/(kg·K))	117 – 1825 (uranium, beryllium)	270 – 1288 (zirconium, boron carbide)	970 – 2000 (PTFE, PEI)	117 - 2000

4.1.3 Initial Design and Analysis Using Box-Behnken

The initial design chosen for this experiment is the Box-Behnken Design (BBD). The BBD generates a spherical design space that excludes the extreme corner points. This is ideal for this DOE, as factor combinations that lie entirely at the extremes of ranges are materially infeasible. For example, no material can have a maximum possible density (21,500 kg/m^3), minimum possible conductivity (0.122 W/ (m·K)), and a maximum possible specific heat (2000 J/(kg·K)). As such, all design points in the BBD are either center points or axial points that contain a midpoint level on at least one factor.

This initial BBD is made up of 13 runs, augmented with the baseline Vascomax observation for a total of 14 observations. Note that there are no repeated center points since this experiment is conducted on a deterministic computer model. Design points are shown in **Table 4.2**. The visualization of the design space is shown in **Figure 4.2**. All designs are generated analyzed using the software tool JMP.

Table 4.2. Initial BBD.

Pattern	Density (kg/m^3)	Conductivity (W/(m·K))	Specific Heat (J/(kg·K))
−0+	1000	210.061	2000
+0+	21500	210.061	2000
0+−	11250	420	117
0−+	11250	0.122	2000
−0−	1000	210.061	117
0	21500	420	1058.5
0++	11250	420	2000
0−−	11250	0.122	117
+0−	21500	210.061	117
−+0	1000	420	1058.5
+−0	21500	0.122	1058.5
0	11250	210.061	1058.5
−−0	1000	0.122	1058.5
Baseline	8000	30.807	857.98

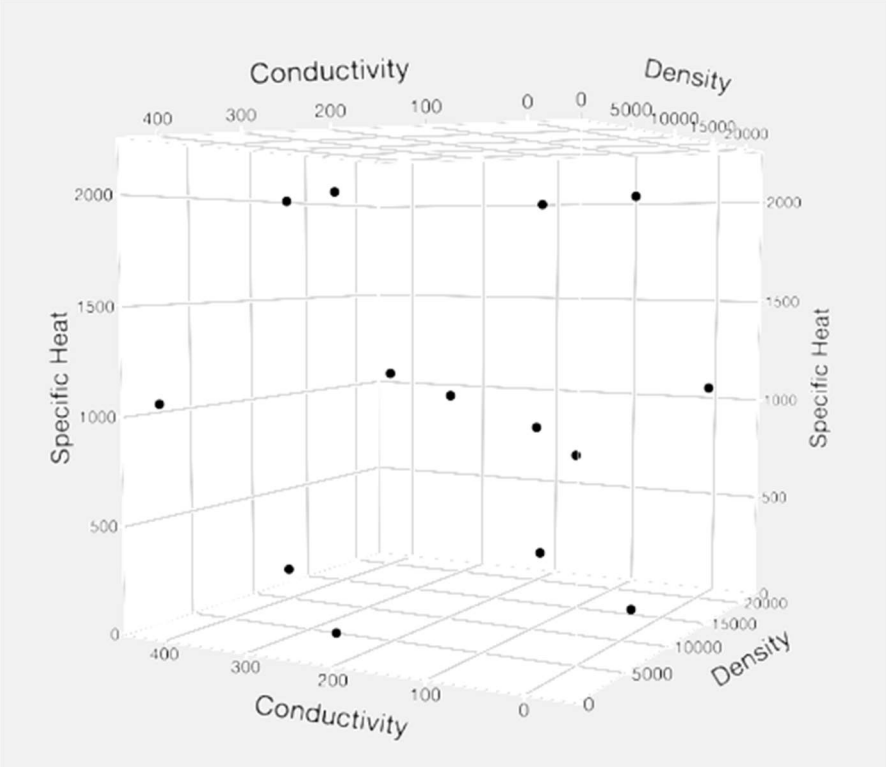

Figure 4.2. 3D visualization of the initial BBD. This design does not contain points on the edges of the design space.

This BBD is built to estimate the response surface as well as all main effects, two-factor interactions, and second order polynomial effects. The average prediction variance of this design is 0.5212, which is moderate. An ideal prediction variance would be very close to zero. **Figure 4.3** shows the correlation map between the effects, with higher correlation marked by darker colors. The diagonal black correlations indicate that each effect is perfectly correlated with itself, as expected. Most correlations on the map are very light, so are not of concern. There is some remarkable correlation between the second order effects density*density (ρ^2), conductivity*conductivity (λ^2), and specific heat*specific heat (c_p^2). However, the map does not indicate these correlations are very severe.

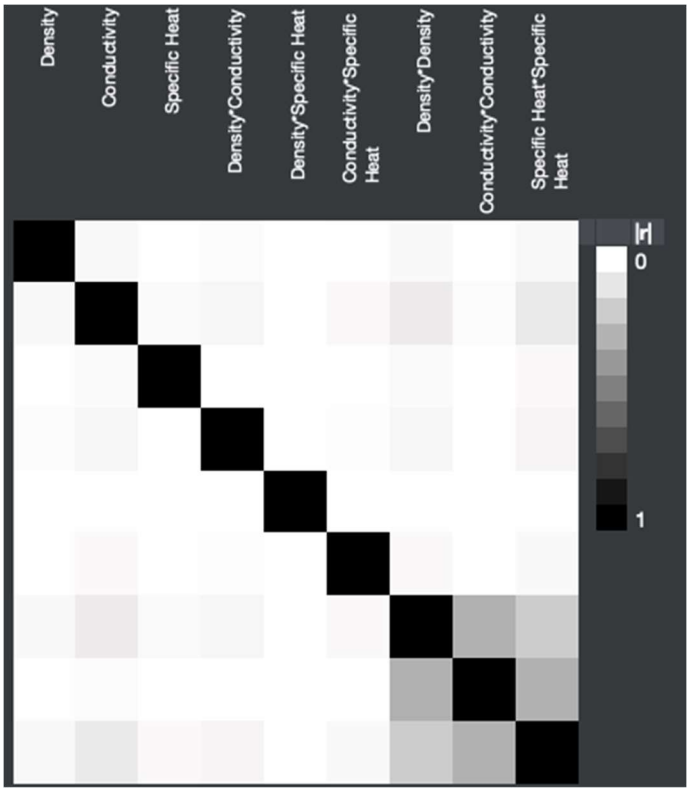

Figure 4.3. Correlation color map of the initial BBD. The black diagonal indicates each effect is perfectly correlated with itself. Less correlation is preferable between effects.

All design points are entered into the 1D transient FEA model in ABAQUS. The responses, measured as maximum change in temperature $\triangle T_{max}$), are recorded from the numeric temperature profile outputs. The design responses are given in **Table 4.3**.

Table 4.3. Initial BBD results.

Run	**Density** kg/m^3	**Conductivity** W/(m·K)	**Specific Heat** J/(kg·K)	$\triangle T_{max}$ K
1	1000	210.061	2000	430.506
2	21500	210.061	2000	218.76
3	11250	420	117	230.761
4	11250	0.122	2000	0.14
5	1000	210.061	117	492.011
6	21500	420	1058.5	192.473
7	11250	420	2000	192.919
8	11250	0.122	117	1647.77
9	21500	210.061	117	426.967
10	1000	420	1058.5	234.06
11	21500	0.122	1058.5	0.135
12	11250	210.061	1058.5	381.144
13	1000	0.122	1058.5	3054.18
Baseline	8000	30.807	857.98	1407.22

These results are fit to a least squares response surface model in JMP, which estimates the response surface along with main effects, two-factor interaction terms, and second order polynomial effects. The prediction expression is as follows:

$$\triangle T_{max} = -0.115317\rho - 6.29024\,\lambda + 0.000352149\rho\lambda + 2368.32,$$

where ρ = density and λ = conductivity. This model indicates that the effects of density*conductivity and conductivity are significant to predicting $\triangle T_{max}$ at a significance level of $\alpha = 0.05$, with p-values of 0.0217 and 0.0284, respectively. The main effect of density is also included in the model because it is a factor within the significant interaction density*conductivity. This maintains model hierarchy. The effects p-value for density of 0.0574

is also quite close to the 0.05 significance level. In terms of fit, this model has moderate predictive capability, with an R^2 value of 0.662 and R^2_{adj} of 0.560. The visualization of the fit is given in the actual vs. predicted plot in **Figure 4.4**.

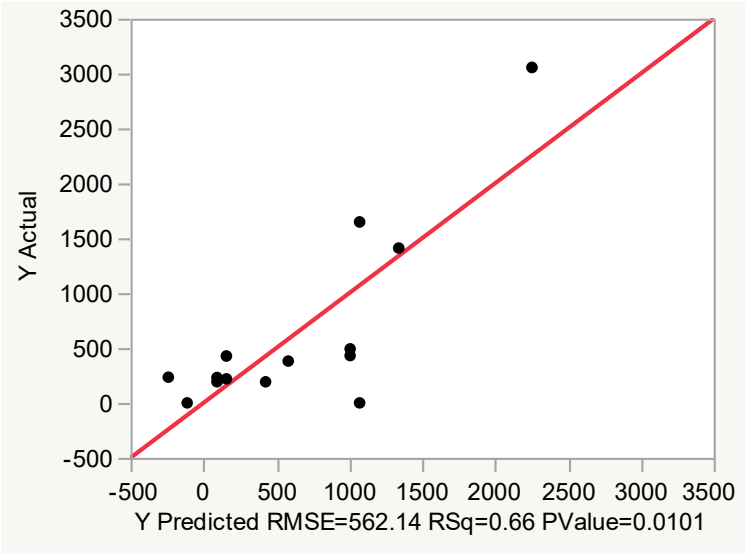

Figure 4.4. Actual vs. predicted plot of initial BBD model.

In terms of model adequacy, the studentized residuals vs predicted values in **Figure 4.5a** do not show any notable structure, indicating it reasonable to assume that residuals are of approximately constant variance. Likewise, residuals fall within a band of the ideal line in **Figure 4.5b**, indicating normal distribution of residuals can be reasonably assumed. The Variance Inflation Factors (VIFs) on the model parameter estimates are all very close to 1, which is ideal. This indicates that the model has no issues with multicollinearity among effects, and that they are independent from one another. Overall, this fitted model is deemed adequate.

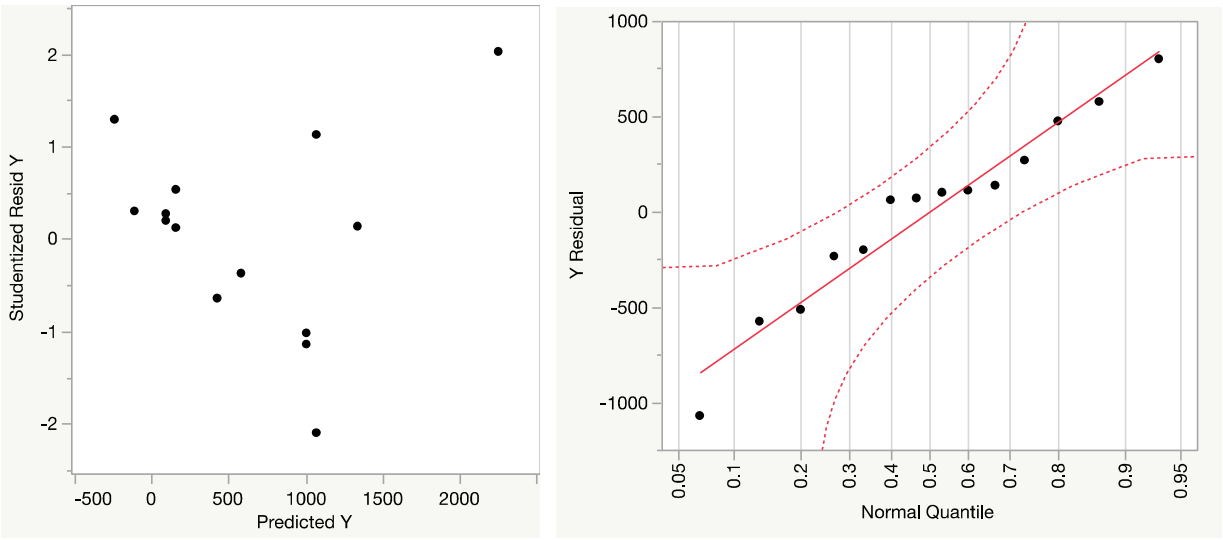

(a) (b)

Figure 4.5. Plots for studentized residuals vs predicted response (a) and normal quantile plot of residuals (b).

In terms of the prediction profile for $\triangle T_{max}$, **Figure 4.6** shows that an optimal maximum temperature change is achieved with density at its low level (1000 kg/m^3) and conductivity at its low level (0.122 W/(m·K)). The predicted $\triangle T_{max}$ at these settings is 2253.58 K above ambient, with a 95% confidence interval of [1362.34, 3144.82], as indicated in the profiler. These temperatures are higher than the melting point of most metals and ceramics, which would indicate that the predominant wear regime would be melt. However, the factor settings at this point are actually only found in engineering plastics, many of which have no known melting point. Therefore, this material is valuable to note for recommendations in potential slipper design.

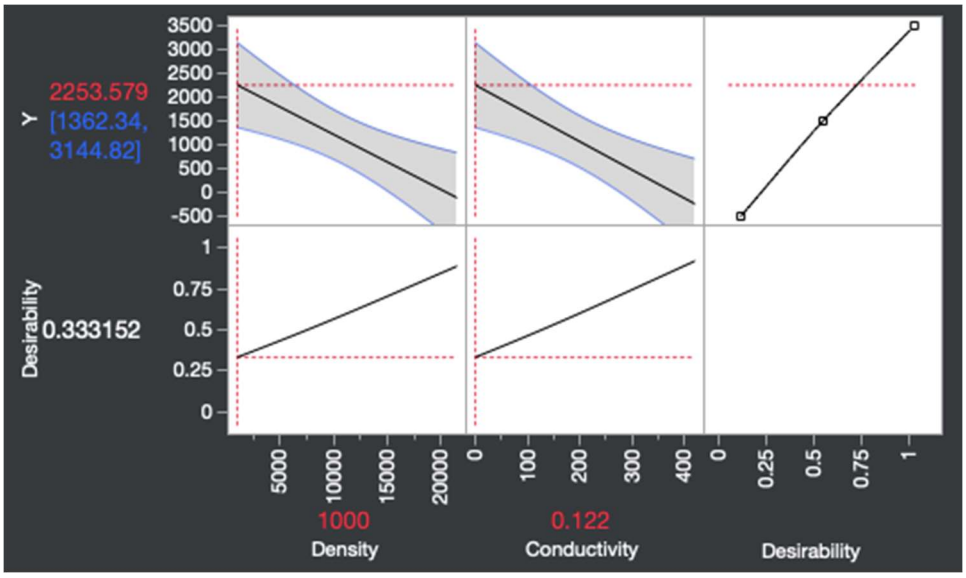

Figure 4.6. Factor settings for optimal (maximum) $\triangle T_{max}$, which rests at levels [density, conductivity] = [-1, -1]. Note desirability is high at these levels.

The minimum response can also be observed to investigate the full range of this experiment. **Figure 4.7** shows that minimal temperature change is achieved at factor settings with density at its low level (1000 kg/m^3) and conductivity at its high level (420 W/(m·K)). However, the predicted $\triangle T_{max}$ is -240.045 K, with a 95% confidence interval of [-1189.1, 709.01] as shown. A negative temperature change is highly unlikely, given what is known about the nature of wear in high-speed environments. In fact, the lower end of the confidence interval is physically infeasible, as it implies a temperature decrease of over 1000K when the starting ambient temperature in the model is 296 K. This decrease would infeasibly put material temperatures below 0 K, or absolute zero.

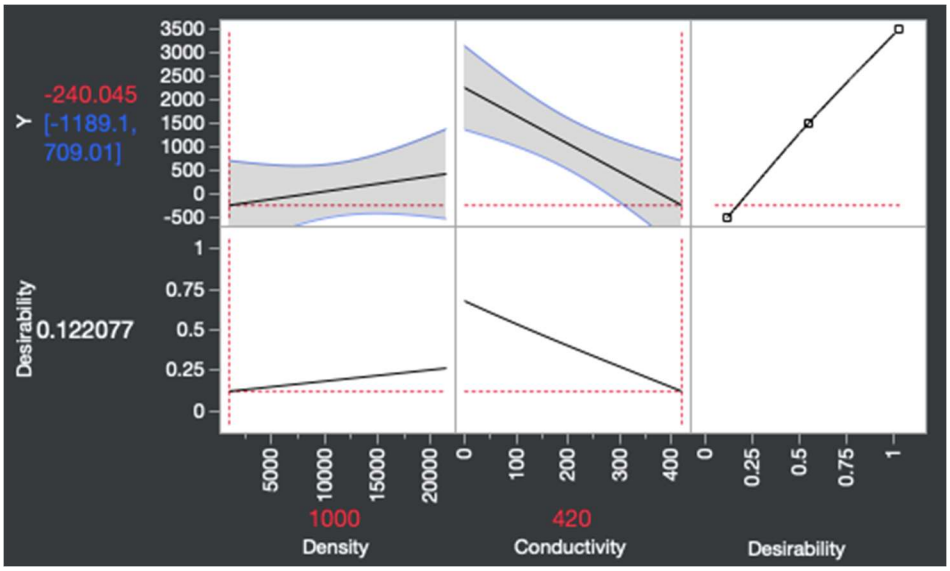

Figure 4.7. Factor settings for minimal $\triangle T_{max}$, falling at levels [density, conductivity] = [-1, 1]. Desirability is low at these levels.

The 3D response surface (**Figure 4.8**) can also be examined to visualize the where optimal designs lie. The model factors conductivity and density lie on the horizontal plane while the response $\triangle T_{max}$ (labelled as Y) lies on the vertical axis. The marked data points are residuals between the model response surface predictions and actual experimental observations. This surface has a saddle shape, with both positive and negative eigenvalues.

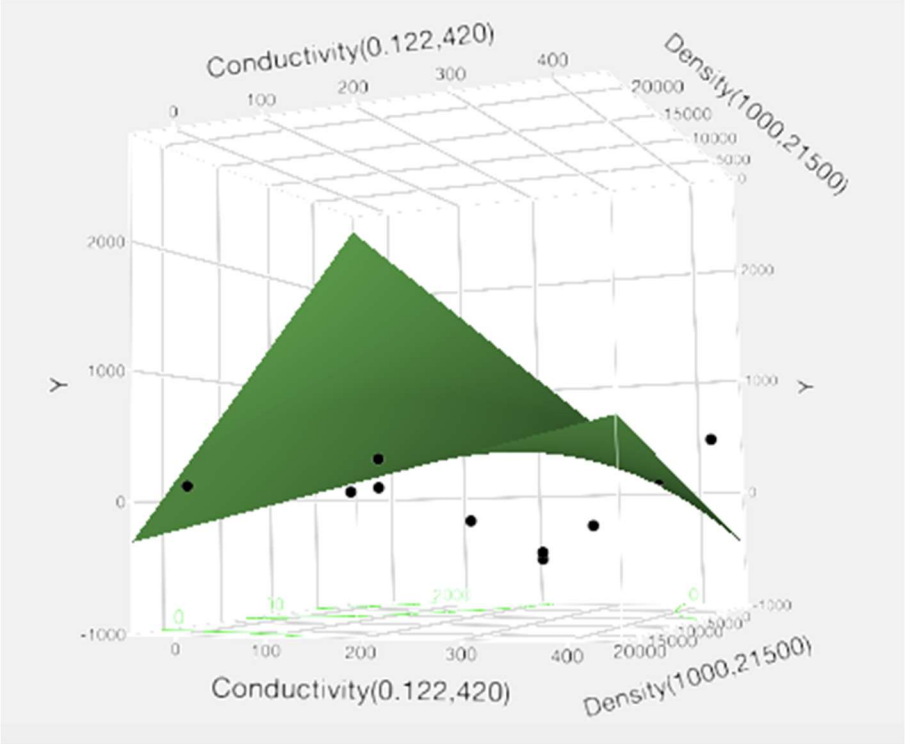

Figure 4.8. Response surface of initial BBD experiment.

The maxima on the response surface lie at factor levels [density, conductivity] = [-1, -1] and [1, 1]. These are visible on the backmost and frontmost areas of the response surface perspective in **Figure 4.8**. The factor setting [-1, -1] corresponds with the global optimum, $\triangle T_{max}$ = 2252.759. The setting [1, 1] corresponds with a local maximum, with a predicted temperature increase of 427.00 K. Despite [1, 1] resting at a local optimum, this value is significantly lower than the baseline temperature change of 1407.22 K. A temperature change of 427.00 indicates an internal temperature of 296 K (ambient) + 427 K = 723 K, which is still significantly lower than melt for most metals and ceramics. Therefore, this point is not ideal.

Minima lie at the far left and right corners of the shown perspective, with [density, conductivity] levels at [1, -1] and [-1, 1], respectively. As indicated in **Figure 4.7**, [-1, 1] is the global minimum in the design region. However, these factor settings both yield response values of $\triangle T_{max} < 0$, which goes against process knowledge of high-speed wear. The local minimum

on the saddle portion of the surface lies at approximately $\rho \simeq 18{,}000$ kg/m^3 and $\lambda \simeq 330$ W/(m·K), yielding a minimum $\triangle T_{max} \simeq 310$ K.

The response minima of this design exhibit concerning behavior that casts doubt on the validity of this model. The global minimum and one local minimum have physically improbable values. This could indicate a few things. It is possible that the original FEA model is not suited to predict the range of material specifications tested in this initial design. It may also be that improbable points on the response surface correlate with factor settings that are not physically possible. While a BBD is specifically chosen to avoid corner points, it is possible that regions at or near the edges of the space are also materially infeasible. These considerations are factored into the next iteration of design.

4.1.4 Process Issues with Initial Design

Other issues during the initial phase of experimentation arise from observation of the FEA model outputs. The baseline design with Vascomax has a temperature profile as shown in **Figure 4.1**, where temperature curves exhibit nearly-linear, mildly oscillating behavior. While many tested design points exhibit similar behavior to this, as shown in **Figure 4.9a**, there are also points that exhibit severely oscillating temperatures as in **Figure 4.9b**.

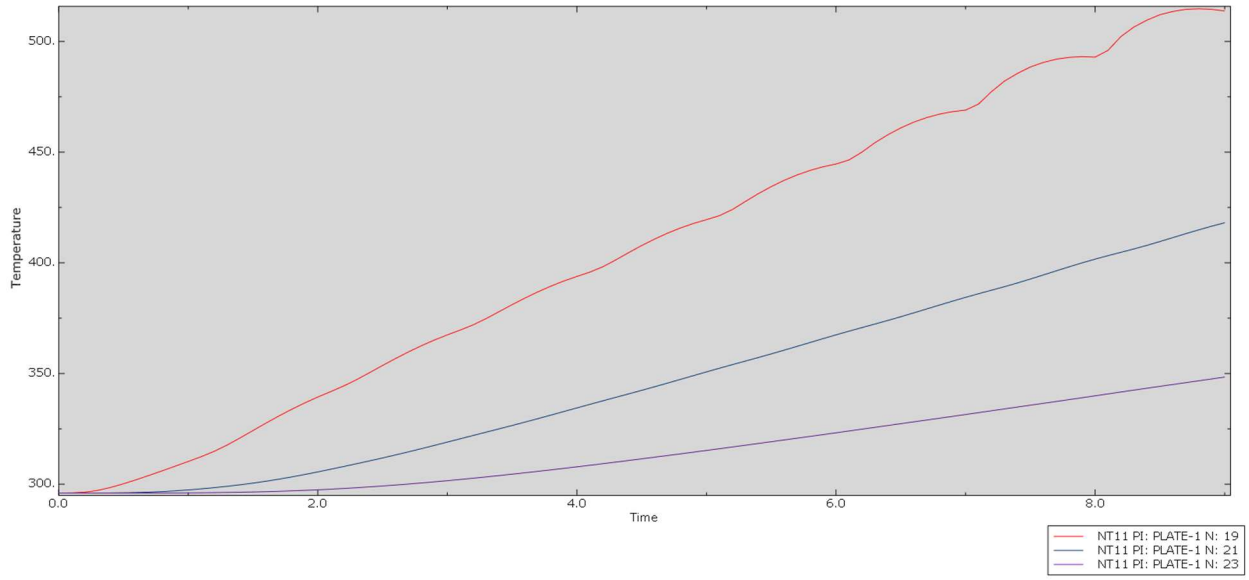

(a)

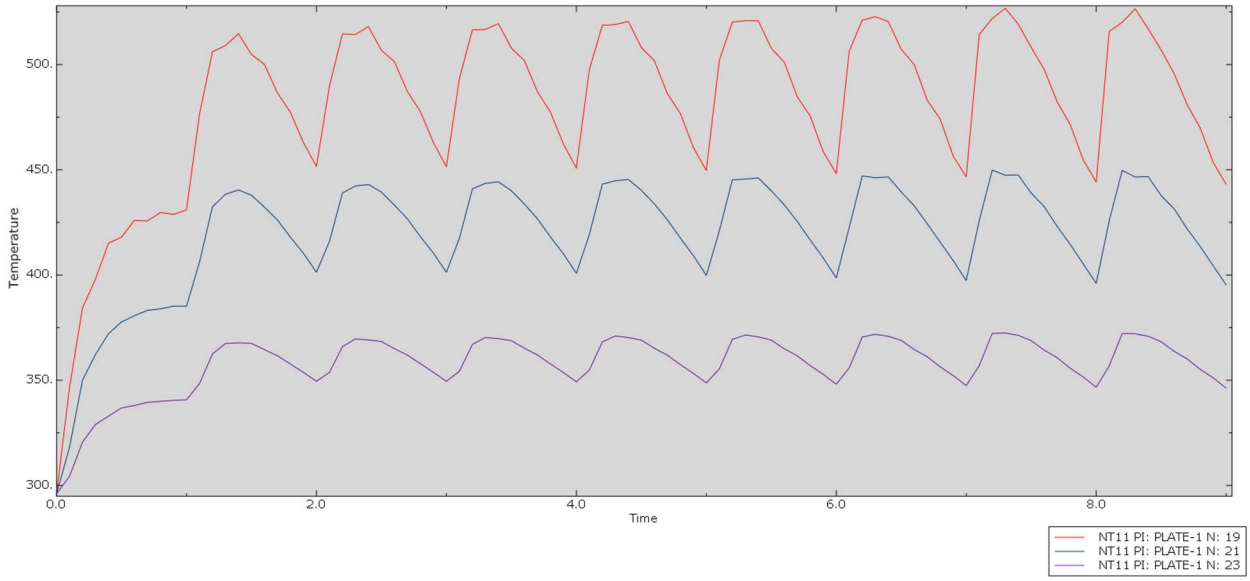

(b)

Figure 4.9. Temperature profile of observation 2 of the BBD (a), exhibiting similar behavior to baseline; and BBD observation 3 (b), exhibiting severely oscillating temperatures.

Severe oscillations are suspected due to numerical computation issues within the FEA, which may be alleviated by decreasing the size of material removal timesteps. The baseline FEA models material displacements in 1-second increments, so a fine-tuned model using timesteps of 0.5 seconds is implemented in ABAQUS 2021 Student Edition. However, the Student Edition cannot execute more than 1000 nodes in the model mesh. The increased number of displacement

timesteps in the fine-tuned model takes up too many nodes at the bottom of the mesh compared to the original FEA, as shown in **Figure 4.10**. Because there are not enough nodes to compute the FEA, this tactic for alleviating oscillations is not executed for this research.

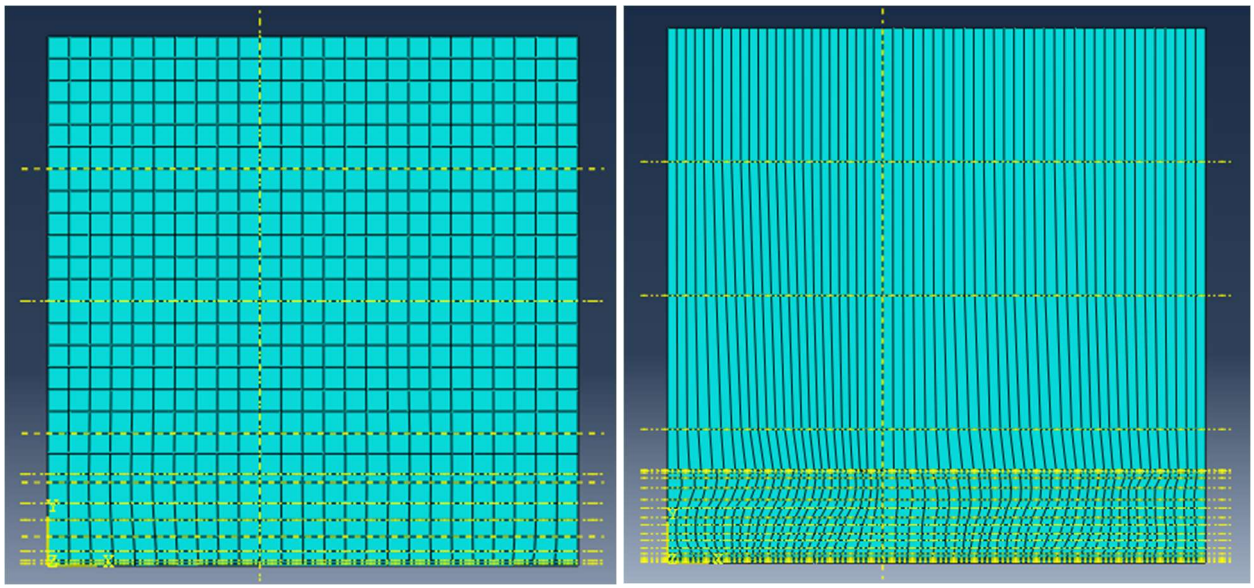

(a) (b)

Figure 4.10. The increased number of material removal steps in (b) compared to (a) does not leave enough nodes to compute temperature flow using FEA.

Instead, temperature profiles with severe oscillations are fit to a smooth least-squares curve. These fitted curves take on the exponential form:

$$f(x) = a(e^{bx}) + c(e^{dx}) \tag{4}$$

The maximum temperature change over the profile $\triangle T_{max}$ is derived from the fitted curve, as shown in **Figure 4.11**. This example is taken from the third BBD run, with parameter estimates as follows:

$$f_3(x) = 496.8(e^{-0.002551x}) - 184(e^{-1.730x})$$

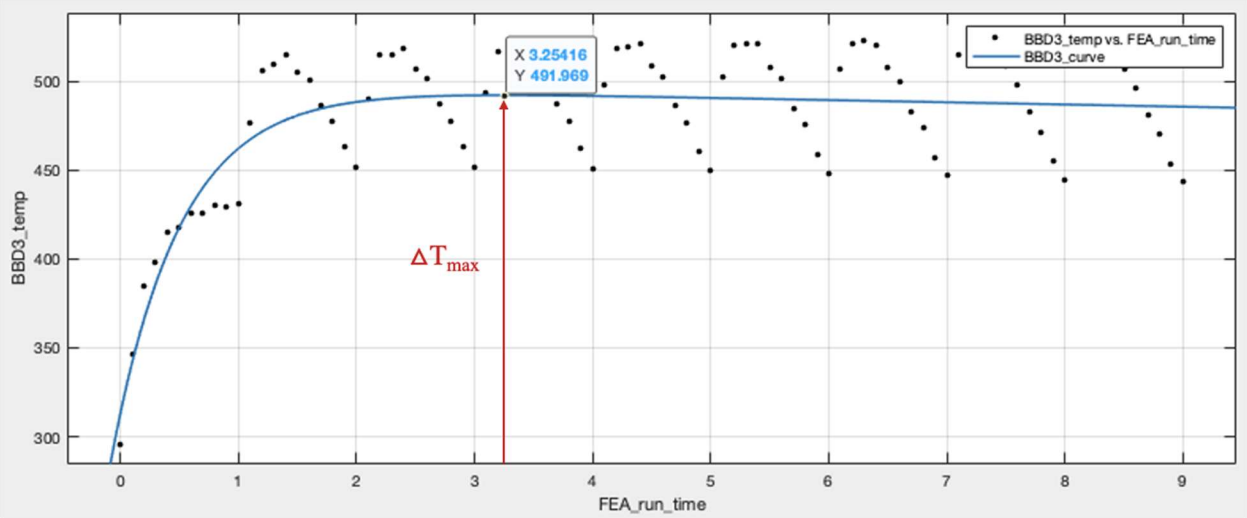

Figure 4.11. Deriving $\triangle T_{max}$ from a fitted least-squares exponential curve on BBD observation 3. $\triangle T_{max}$ in this example lies at 491.969 K – 296 K (ambient) = 195.969 K.

Another family of concerning temperature profiles exhibits highly exponential behavior, as shown in **Figure 4.12**. These observations are concurrent with designs in which specific heat lies at the low level (c_p = 0.122). These observations are concerning because they are often associated with extreme responses: observations 4 and 11 in **Table 4.3** result in a maximum temperature change of less than a single Kelvin, while observation 13 results in a maximum temperature change of over 3000 K.

These exponential profiles also exhibit drastically differing temperatures between the three thermocouples. In fact, temperatures for thermocouples 2 and 3 are so small relative to thermocouple 1 that only thermocouple 1 is visible on these graphs, as shown in **Figure 4.12**.

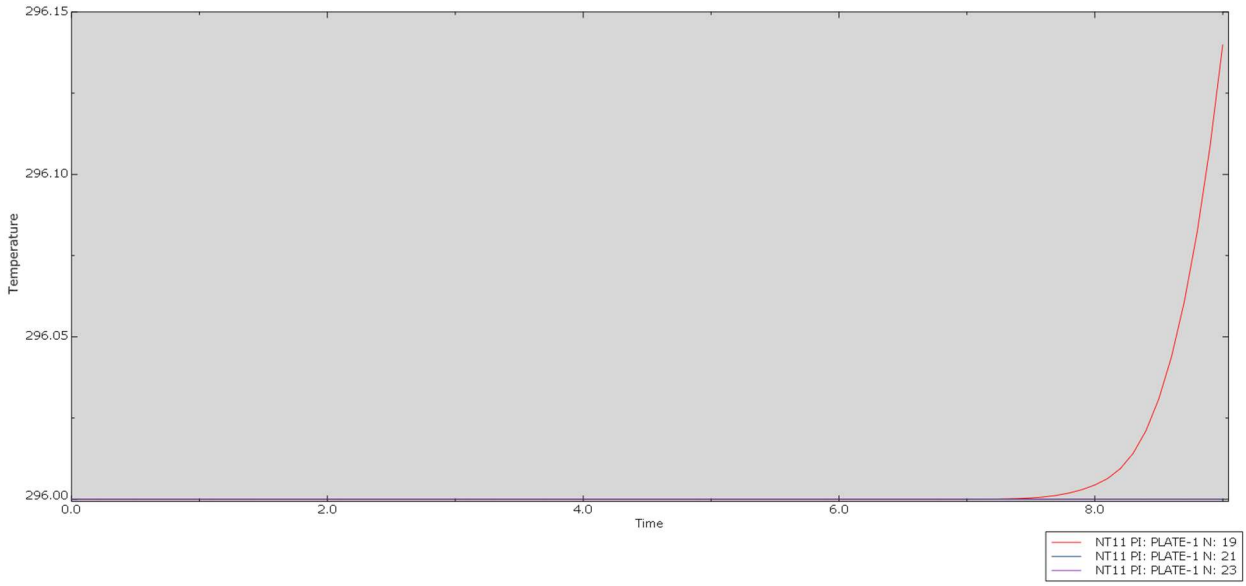

Figure 4.12. Temperature profile of observation 4, exhibiting exponential behavior in one thermocouple, temperatures do not increase above ambient 286 K in thermocouples 2 and 3.

Overall, the behavior of these observations is drastically different from that of the baseline material. This casts doubt on whether the applied factor settings are a) materially feasible, and b) able to be modeled with validity within the FEA. These issues are again taken into consideration in the next phase of experimentation. The problem of potentially infeasible observations in particular indicates that a BBD is insufficient to generate an accurate response surface. While the BBD is made up of axial points along the edge of the cube and a single center point, it is necessary to augment this experiment with more points inside the region and to discard any infeasible points.

4.2 Improved Design and Analysis

Results from initial experimentation using the BBD indicate that not all axial points in the factor space are materially feasible. The next step of design is to then conduct experimentation using the same response and factors, but on an updated design space. The updated space blocks off materially infeasible regions, and the feasible region is filled with near-evenly spaced design

points in a Space Filling Design (SFD). Because the region is non-rectangular, a Flexible Fast Filling Design (FFFD) type of SFD is implemented.

4.2.1 Determination of Improved Design Space

The first step in this phase is to narrow down the design space by blocking off materially infeasible regions. The approximate regions of feasibility based off of **Table 4.1**'s specifications are shown in **Figure 4.13**. While it is possible to simply block off all areas outside of each region, this does not leave room for potential composites. Composites are materials made out of two or more materials with different properties (Williams). For the purposes of this research, only two-material composites are considered.

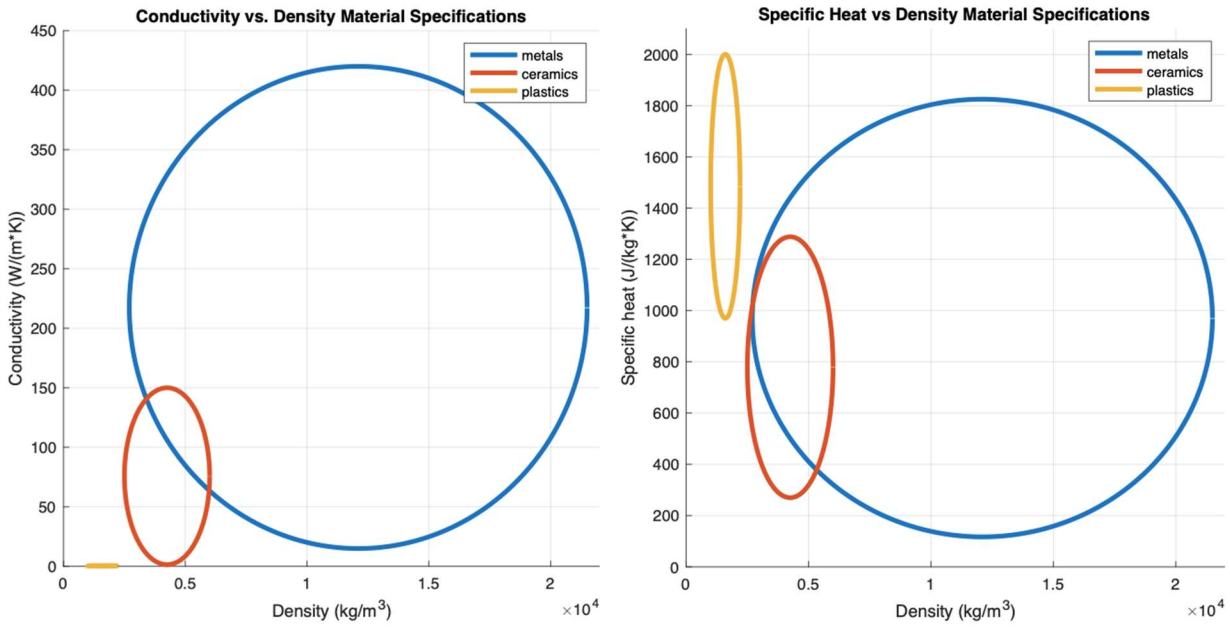

(a) (b)

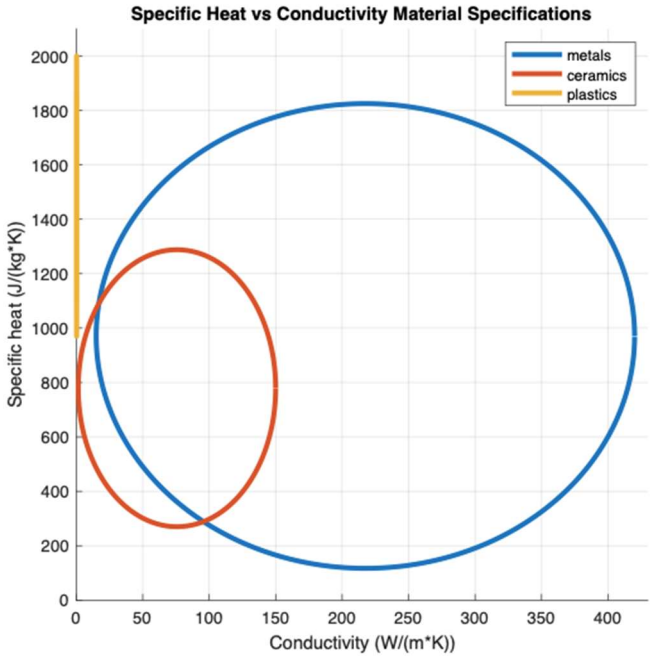

(c)

Figure 4.13. Material specification range for (a) density and conductivity, (b) density and specific heat, and (c) conductivity and specific heat.

Composites are important to consider because they can combine useful features of multiple materials. For example, mud bricks reinforced with straw have good compressive strength from mud as well as good tensile strength from straw (Williams). Composites can also

increase the magnitude of strength, such as a graphene-copper composite that produces a material 500 times stronger than copper individually. Many composites are also tailored to produce materials with ideal heat conduction or insulation properties (Williams).

In terms of density, thermal conductivity, and specific heat relating to composites, there is generally a normalizing effect between specification values. That is, the specifications of composites lie somewhere between the individual specifications that make up the material.

For example, the Ashby chart in **Figure 4.14** shows how polymer-metal composite densities lie roughly in the middle of polymer densities and metal densities. Polymers are materials composed of large macromolecules, which include engineering plastics such as PEEK and HDPE as well as nylons (Ayers).

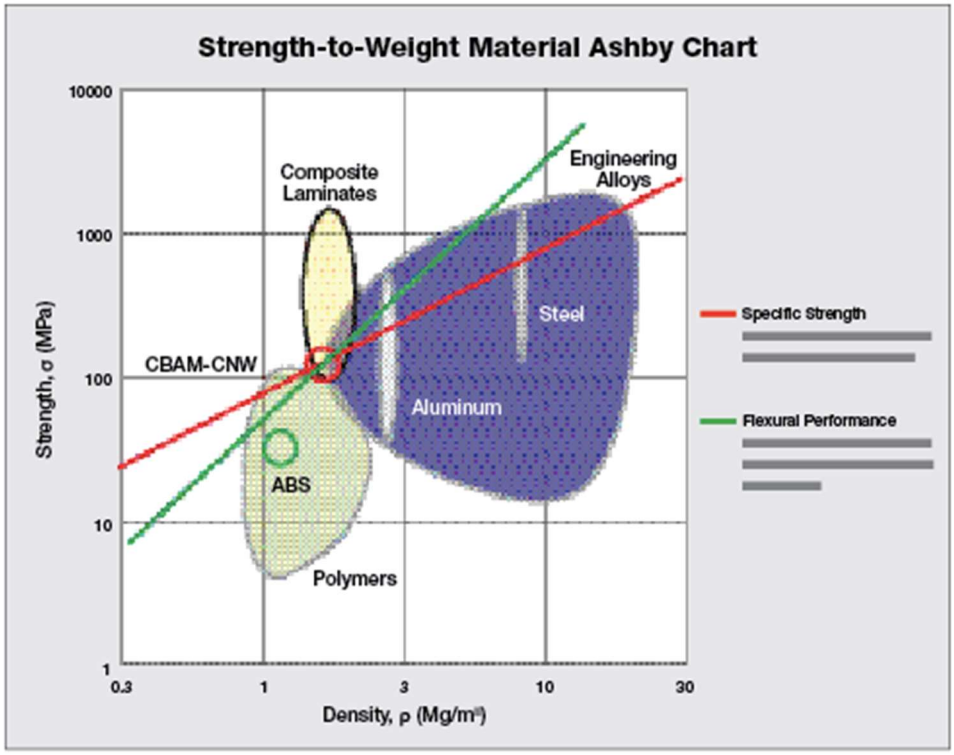

Figure 4.14. Normalization of densities between plastic and metal composites (Ayers).

Similarly, the thermal conductivity and specific heat of composites tend to lie in between those of the individual components. **Figure 4.15** shows the relationship between the thermal

conductivity value and the % AgNP silver within a PEEK thermoplastic composite. **Figure 4.16** shows the specific heat relationship for this composite. In general, the specification values lie in between those of AgNP and PEEK (Rivière, Causse and Lonjon).

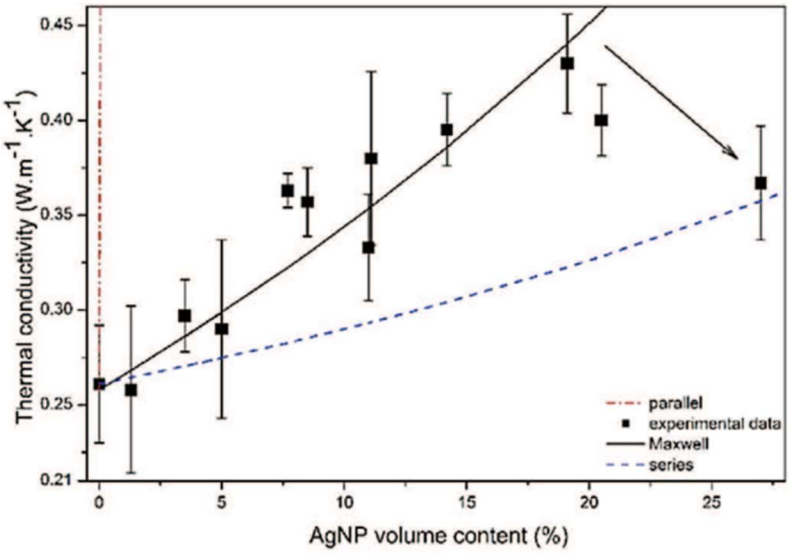

Figure 4.15. Relationship between thermal conductivity and AgNP content within a PEEK/AgNP composite (Rivère, Causse, and Lonjon).

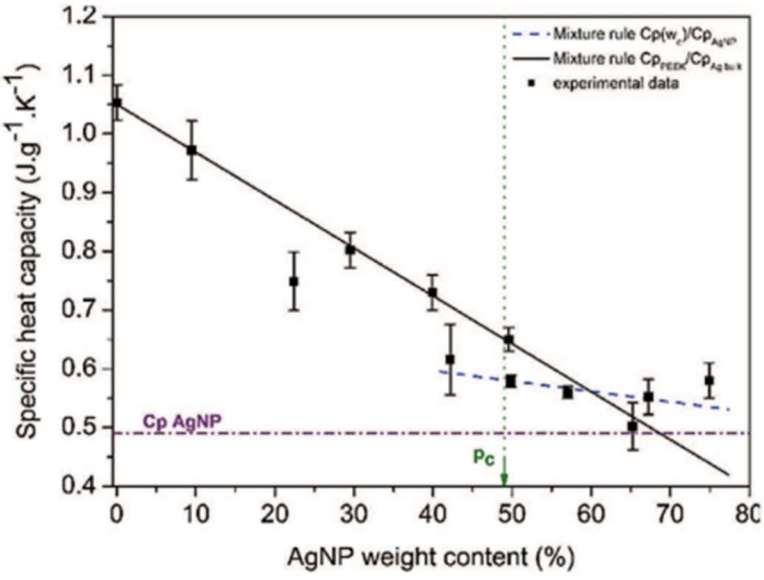

Figure 4.16. Relationship between specific heat and AgNP content within a PEEK/AgNP composite (Rivère, Causse, and Lonjon).

As shown in **Figure 4.16**, the relationship between material proportion in a composite and the specification value is not always linear, so a conservative approximation of a feasible

design space is taken. This is to avoid blocking off areas that may be feasible. It is always possible to generate an observation and remove it later upon finding it infeasible, but it is more difficult to determine new points to generate upon already having completed design and experimentation.

To determine the design space, infeasible regions are approximated. The method for approximation is as follows: for each material specification pair as in **Figure 4.13**, determine the extreme (boundary) specifications for any given material, then generate bounds of infeasibility using midpoints. For example, when observing conductivity (λ) vs. density (ρ), the lower bound for ρ is found in plastics. Composite behavior and **Figure 4.13** (a) indicate that a material with densities in this low region of ρ must be predominantly if not all plastic. Conversely, materials with λ in the upper boundary range of must be predominantly if not all metal. Therefore, it is very unlikely for a material to assume both specifications of extremely low ρ and extremely high λ.

To account for potential composites between plastics, ceramics, and metals, an approximation is made that no material can assume specifications where ρ falls below the midpoint of ρ's lower bounds (1000 for plastics and 2500 for ceramics), while λ simultaneously rests above the midpoint of λ's upper bounds (150 for ceramics and 420 for metals). This equates to ruling that no material can have a $\rho < 1750$ and a $\lambda > 285$. This process is repeated for the converse boundaries (upper bounds for ρ and lower bounds for λ), and for all three specification combinations. The approximated region of infeasibility for the λ vs. ρ example is shown in **Figure 4.17**.

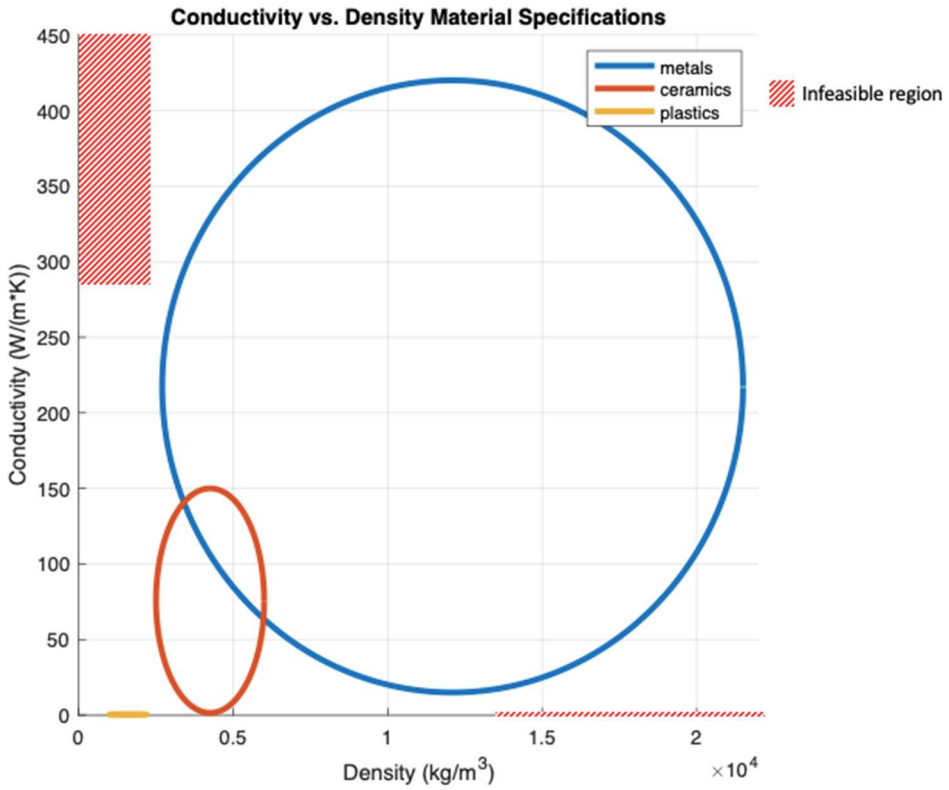

Figure 4.17. Infeasible combinations for conductivity and density.

This process for estimating infeasible regions is repeated for specific heat c_p vs ρ, and c_p vs λ. These regions are given in **Table 4.4**.

Table 4.4. Infeasible combinations in SFD design space.

Combination	Infeasible 1	Infeasible 2
ρ & λ	$\rho < 1750$ & $\lambda > 285$	$\rho > 13{,}750$ & $\lambda < 0.811$
c_p & λ	$c_p < 193.5$ & $\lambda < 0.811$	$c_p > 1912.5$ & $\lambda > 285$
c_p & ρ	$c_p < 193.5$ & $\rho < 1750$	$c_p > 1912.5$ & $\rho > 13{,}750$

4.2.2 Analysis of Space-Filling Design using Response Surface Method

Using the updated design space, a Fast-Flexible Filling Design (FFFD) type of Space-Filling Design (SFD) is generated. The FFFD near-evenly spreads design points throughout the non-rectangular design space using the maximum projection (MaxPro) criterion.

The FFFD is made up of 15 runs, augmented with 5 viable design points from the BBD and the baseline Vascomax for a total of 21 observations. The MaxPro value of the FFFD is

$C_{MaxPro} = 18.7843$. The full design for this phase is shown in **Table 4.5**, and visualization of design points is shown in **Figure 4.18**.

Table 4.5. Augmented SFD.

Observation	**Density** kg/m^3	**Conductivity** W/(m·K)	**Specific heat** J/(kg·K)
SFD1	21394.6107	7.41683103	166.40989
SFD2	13682.8142	80.028082	1952.41725
SFD3	20055.7326	142.487369	1345.72045
SFD4	20962.2328	397.82461	1847.77728
SFD5	15120.1517	419.58395	314.172811
SFD6	1828.99384	409.783324	910.815775
SFD7	9407.53905	122.430071	271.332988
SFD8	16571.4374	219.575883	820.576009
SFD9	19256.7348	330.967448	514.768525
SFD10	1091.30096	1.10786968	1661.33804
SFD11	8375.76193	359.959705	1521.19419
SFD12	11324.0565	245.409138	1751.04734
SFD13	6654.43585	27.3940272	648.897563
SFD14	5220.38412	178.653464	1162.05168
SFD15	3783.62058	273.861328	137.856523
BBD1	1000	210.061	2000
BBD3	11250	420	117
BBD6	21500	420	1058.5
BBD9	21500	210.061	117
BBD12	11250	210.061	1058.5
Baseline	8000	30.807	857.98

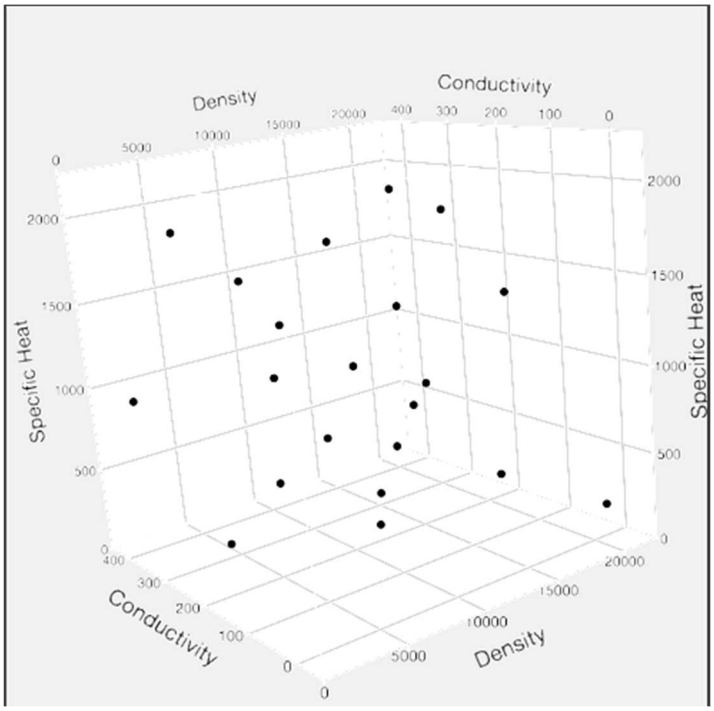

Figure 4.18. 3D visualization of the augmented SFD.

These observations are used to estimate the response surface as well as all main effects, two-factor interactions, and second order polynomial effects. SFD design points are entered into the FEA model in ABAQUS to generate unique temperature profiles. The responses $\triangle T_{max}$ are recorded from the numeric temperature profile outputs and given in **Table 4.6**. In cases where the profile exhibits severe oscillation, determined as when a curve drawn through the oscillations does not monotonically increase, the fitted least squares approach described in equation (4) **Section 4.1.4** is applied to estimate $\triangle T_{max}$. Of these tested 21 design points, the baseline Vascomax performs better than 0.773 of results, or in the 77th percentile.

Table 4.6. Augmented SFD results.

Observation	Density (kg/m^3)	Conductivity (W/(m·K))	Specific heat (J/(kg·K))	$\triangle T_{max}$ (K)
SFD1	21394.6107	7.41683103	166.40989	3426.42
SFD2	13682.8142	80.028082	1952.41725	414.801
SFD3	20055.7326	142.487369	1345.72045	338.083
SFD4	20962.2328	397.82461	1847.77728	169.94
SFD5	15120.1517	419.58395	314.172811	200.0196
SFD6	1828.99384	409.783324	910.815775	201.7625

SFD7	9407.53905	122.430071	271.332988	683.8543
SFD8	16571.4374	219.575883	820.576009	357.055
SFD9	19256.7348	330.967448	514.768525	262.003
SFD10	1091.30096	1.10786968	1661.33804	7288.4
SFD11	8375.76193	359.959705	1521.19419	238.249
SFD12	11324.0565	245.409138	1751.04734	295.229
SFD13	6654.43585	27.3940272	648.897563	1955.79
SFD14	5220.38412	178.653464	1162.05168	481.592
SFD15	3783.62058	273.861328	137.856523	298.474
BBD1	1000	210.061	2000	399.0753
BBD3	11250	420	117	195.9702
BBD6	21500	420	1058.5	192.473
BBD9	21500	210.061	117	399.7829
BBD12	11250	210.061	1058.5	381.144
Baseline	8000	30.807	857.98	1407.22

These results are fit to a response surface model in JMP. Once again using a significance level of $\alpha = 0.05$, the prediction expression for this model is as follows:

$$\triangle T_{max} = 0.0000109\rho^2 - 0.295\rho + 0.0414\lambda^2 - 24.882\lambda + 5024.160,$$

This model indicates that the effects of conductivity and conductivity^2 are significant to predicting $\triangle T_{max}$ below the level of α = 0.05, with p-values of 0.00015 and 0.00348 respectively. The second order effect density^2 is on the border of the significance level, with an effects p-value of 0.0517. Maintenance of model hierarchy dictates that the main effect of density (p-value = 0.130) should also be kept if including density^2. It is found that the model including the density terms yields an R^2_{adj} of 0.661 compared to an R^2_{adj} of 0.587 without, so the higher term model is kept. This higher term model has overall good predictive capability, with an R^2 value of 0.728. The visualization of the fit is given in the actual vs. predicted plot in **Figure 4.19**.

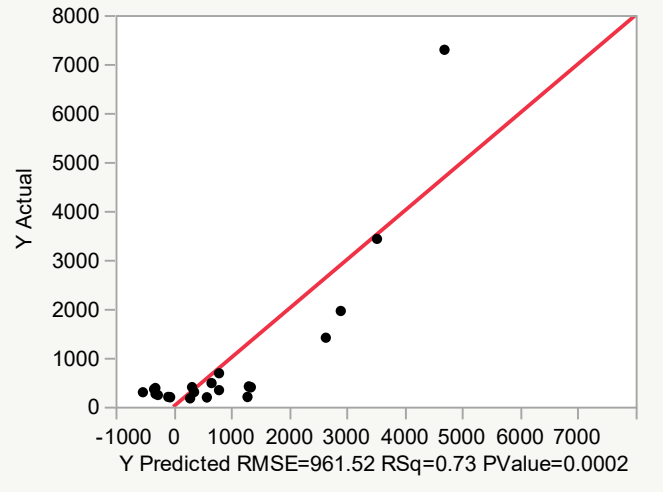

Figure 4.19. Actual vs. predicted plot of augmented SFD model.

In terms of model adequacy, the studentized residuals vs row number in **Figure 4.20** indicate a potential issue with observation 10. Ideally, residuals should fall approximately within a horizontal band, as indicated by the red 95% Bonferroni limits. However, observation 10 lies well outside of this band. This observation is associated with the largest $\triangle T_{max}$ of 7288.4 K. While this in itself does not present an issue, the Cook's D value of this observation is 2.193, which is above the ideal value of 1.00. This indicates the observation is likely an outlier, and may exert undue influence on the model. The model is thus rerun with observation 10 removed. The resulting model's significant effects (maintaining hierarchy) and p-values are given in **Table 4.7**.

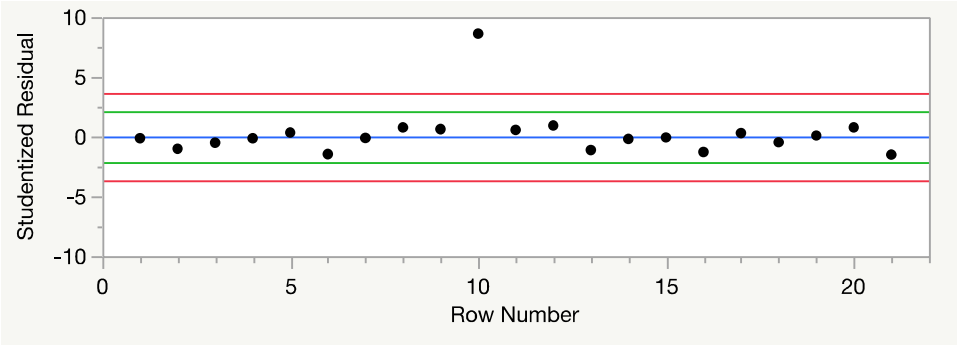

Figure 4.20. Studentized residuals indicate abnormality in observation 10.

Table 4.7. Model effects with observation 10 removed.

Effect	**p-value**
Conductivity	0.00001
Conductivity*Conductivity	0.00011
Conductivity*Specific Heat	0.00276
Specific Heat	0.02619
Density*Specific Heat	0.02767
Density	0.61662

This rerun model is significant with a large F-statistic of 29.290 and a good fit with R^2 = 0.918; however, the same issue with model adequacy appears. **Figure 4.21** shows that observation 1 contains studentized residuals that fall outside of an approximately horizontal band. Cook's D influence value on this observation is 2.240, which again falls above the ideal of 1.00.

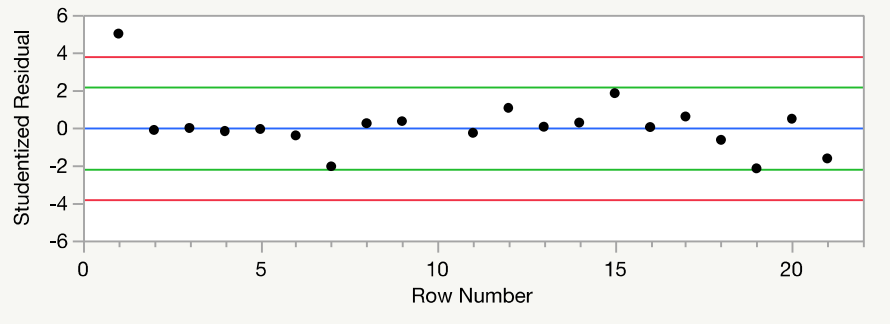

Figure 4.21. Studentized residuals indicate abnormality in observation 1.

It is notable that barring observation 10, this observation corresponds with the next highest $\triangle T_{max}$ of 3426.42 K. Since the goal for this problem is to maximize $\triangle T_{max}$, it is problematic that the regression model treats these high values as outliers.

Removal of this observation confirms this trend: the rerun model excluding both observations 10 and 1 gives that observation 13, corresponding with the next highest $\triangle T_{max}$ of 1955.79 K, is considered an outlier. This is especially concerning given that this value is not far off from the baseline Vascomax $\triangle T_{max}$ of 1409.58 K. Even though the studentized residual for

observation 13 once again falls above the Bonferroni limit and the Cook's D is 1.3110, it would be tenuous to remove this observation from consideration.

This raises the issue that a second-order response surface model may not be able to capture the highly nonlinear behavior of this data. It is suspected that there may be higher order terms, such as third or fourth order polynomials, that better capture the behavior of the data. In the next phase, a Gaussian process approach is taken to assess and model the data.

4.2.3 Analysis of Space-Filling Design using Gaussian Process

The Gaussian process is applied to obtain a higher resolution estimation of the data. Instead of a second-order model, the data is interpolated using weights. The same FFFD design points as in **Table 4.6** are loaded into JMP. Two approaches to the Gaussian process are taken: with and without estimating the nugget parameter. The nugget is a parameter that can be useful to include in model estimation when there is high noise or randomness in the data. **Figure 4.22** shows that the model sans nugget parameter estimation provides a better actual vs predicted plot, with very similar log-likelihood values (344.781 with nugget and 345.127 sans nugget). As such, the no-nugget parameter estimation model is taken.

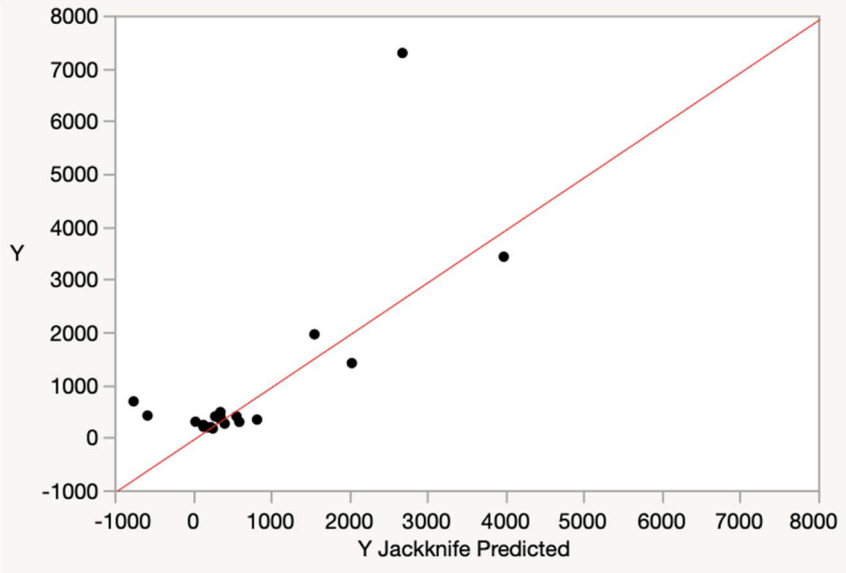

(a)

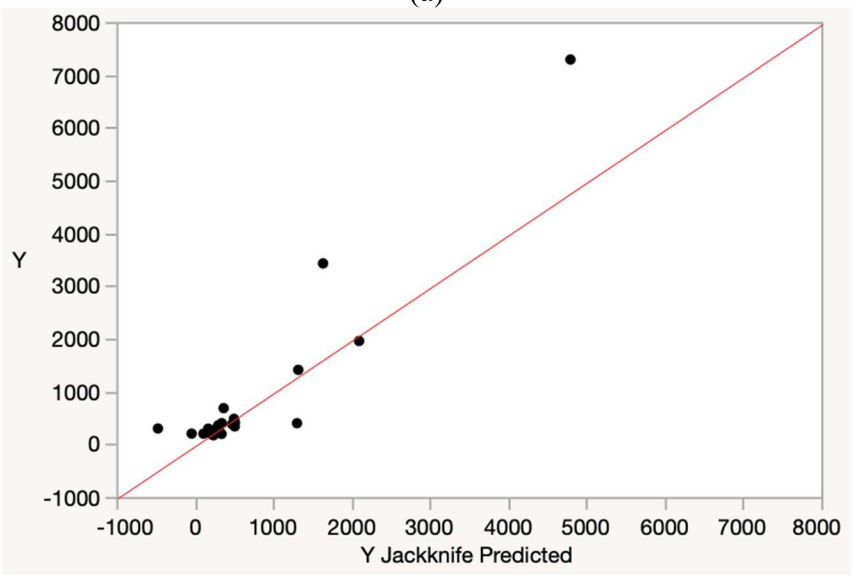

(b)

Figure 4.22. Actual vs predicted plots with (a) and without (b) nugget parameter estimation. The plot for (b) is closer to the ideal 45-degree line in red.

The mean response value given by this Gaussian process model is $\mu = 3808.802$ K while $\sigma = 4126.083$, which is a considerably large spread. The parameter estimates for the model are given by the theta values in **Table 4.8**.

The Gaussian process model estimates that conductivity has the highest impact on the $\triangle T_{max}$ response with a total sensitivity value of 0.866. Density is also a significant predictor to the response, while the impact of specific heat is negligible. The sensitivity from conductivity

comes approximately 61% from the main effect and 39% from the conductivity*density interaction. Density effects are derived approximately 25% from the main effect and 75% from the conductivity*density interaction.

Table 4.8. Parameter estimates for Gaussian process model.

Effect	Theta	Total Sensitivity	Main Effect	Density Interaction	Conductivity Interaction	Specific Heat Interaction
Density	4.81E-09	0.4474842	0.1097304	.	0.3361762	0.0015775
Conductivity	0.000011	0.8658509	0.5270687	0.3361762	.	0.002606
Specific Heat	9.03E-09	0.0190658	0.0148823	0.0015775	0.002606	.

The impact of each main effect on the response can also be visualized using marginal model plots, as shown in **Figure 4.23**. The plots for density and conductivity display curvature that flattens out toward the higher ends of the respective ranges. Specific heat does not display notable curvature. The plot also lies very flat, indicating it has little leverage on the response.

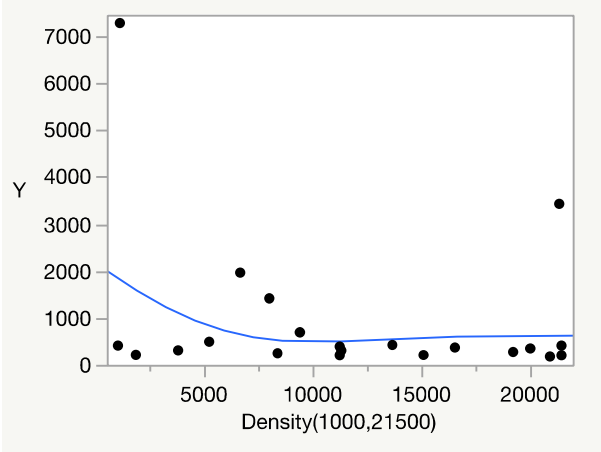

(a)

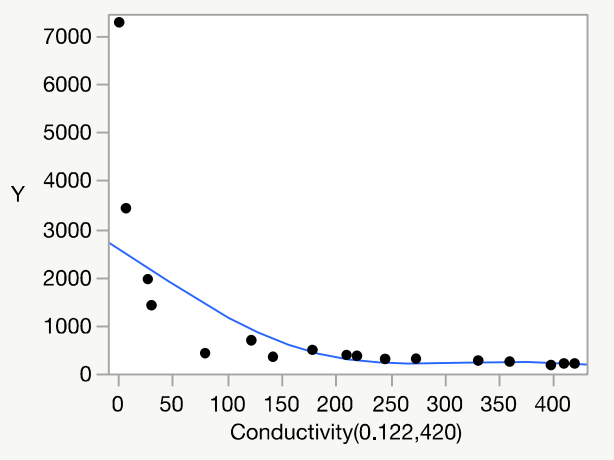

(b)

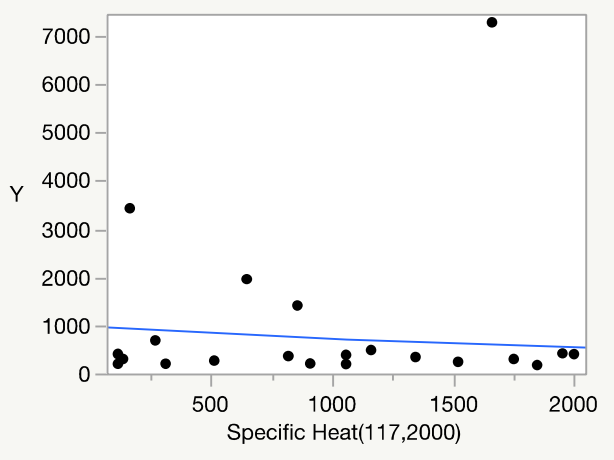

(c)

Figure 4.23. Marginal model plots of $\triangle T_{max}$ response (labelled "Y") vs main effects density (a), conductivity (b), and specific heat (c).

This Gaussian process model is used to determine optimal material specifications for slipper design. The surface profile of the response $\triangle T_{max}$ (labelled as "Y" on the z-axis) compared to significant effects conductivity and density can be viewed in **Figure 4.24**. The surface displays highly nonlinear behavior, with flared 'wings' of higher $\triangle T_{max}$ toward the edges of the space at [conductivity, density] levels of [-1, 1], [1, -1], and [-1, -1]. As shown, the highest increase occurs at the low levels [-1, -1] of conductivity and density.

The factor profiler shown in **Figure 4.25** also provides visualization of the model prediction. Maximizing desirability on this profile gives an estimated $\triangle T_{max}$ of 7565.931 K,

with a 95% confidence interval [7397.35, 7734.51]. As supported by the surface profiler, this optimal response is achieved at factor settings [conductivity, density, specific heat] = [-1, -1, 1]. **Figure 4.25** also shows significant curvature in the conductivity and density factors, while specific heat displays very little impact on the response. This elaborates on the parameter estimates given in **Table 4.8** and confirms the behavior in the marginal model plots given in **Figure 4.23**.

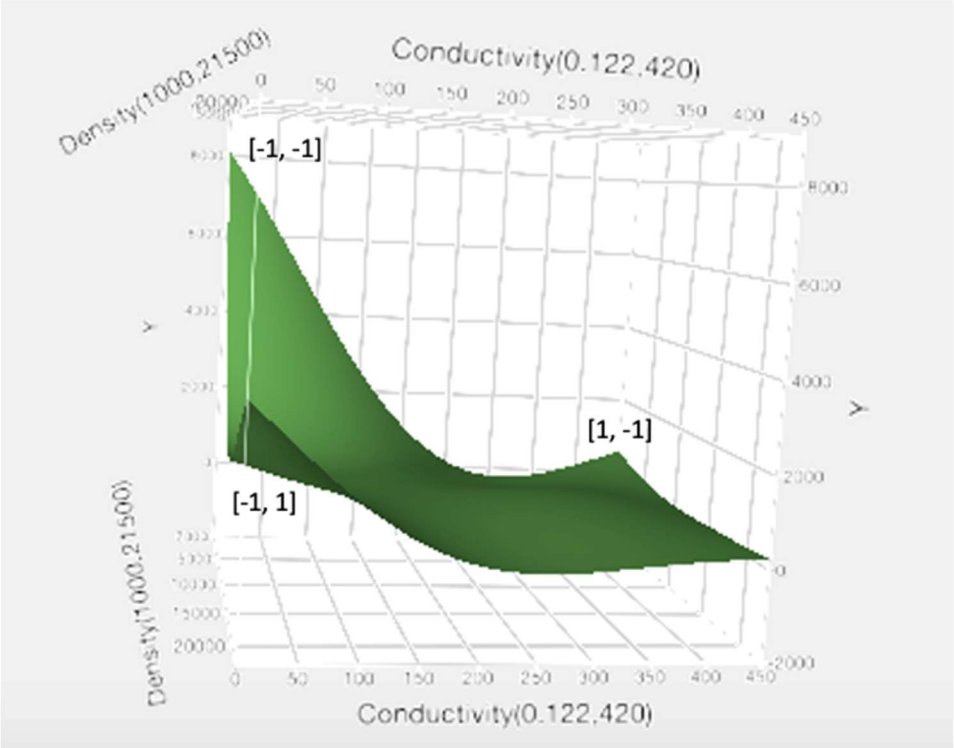

Figure 4.24. Surface profiler of Gaussian process model.

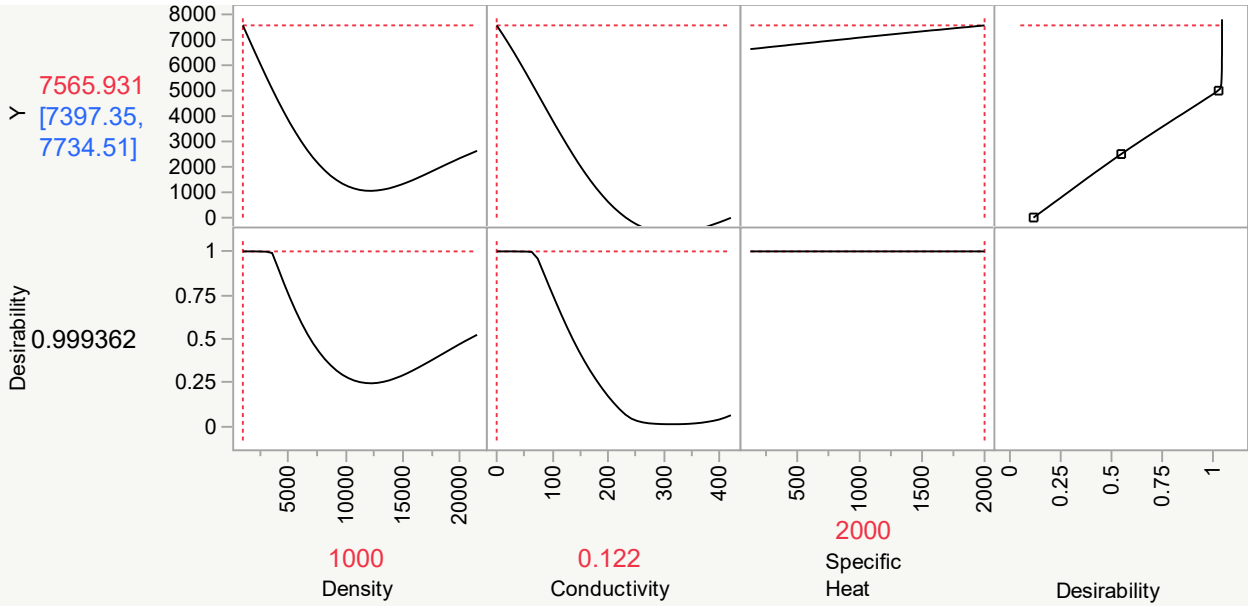

Figure 4.25. Factor profiler for the Gaussian process model set at maximum desirability (maximum $\triangle T_{max}$).

Potentially the most useful output from this Gaussian process model is the contour profiler given in **Figure 4.26**. For materials design, it is not always possible or preferable to simply pick the precise specification levels that give the maximum possible output. Contour plots can show factor regions where the response may not be at absolute optimal, but values are close to ideal or more ideal than the current baseline design.

The contour lines represent response values for $\triangle T_{max}$ on a profile looking at the two most significant factors, conductivity and density. The baseline design with Vascomax maraging steel has a response value of 1409.58 K. Regions on the plot that yield contour lines near or above this baseline response are of interest. This approximate region is shaded in green in **Figure 4.26**, with areas yielding a $\triangle T_{max}$ greater than ~1300 K being of interest. The contour identifies that in general, materials with low conductivity and very high or very low densities are of interest.

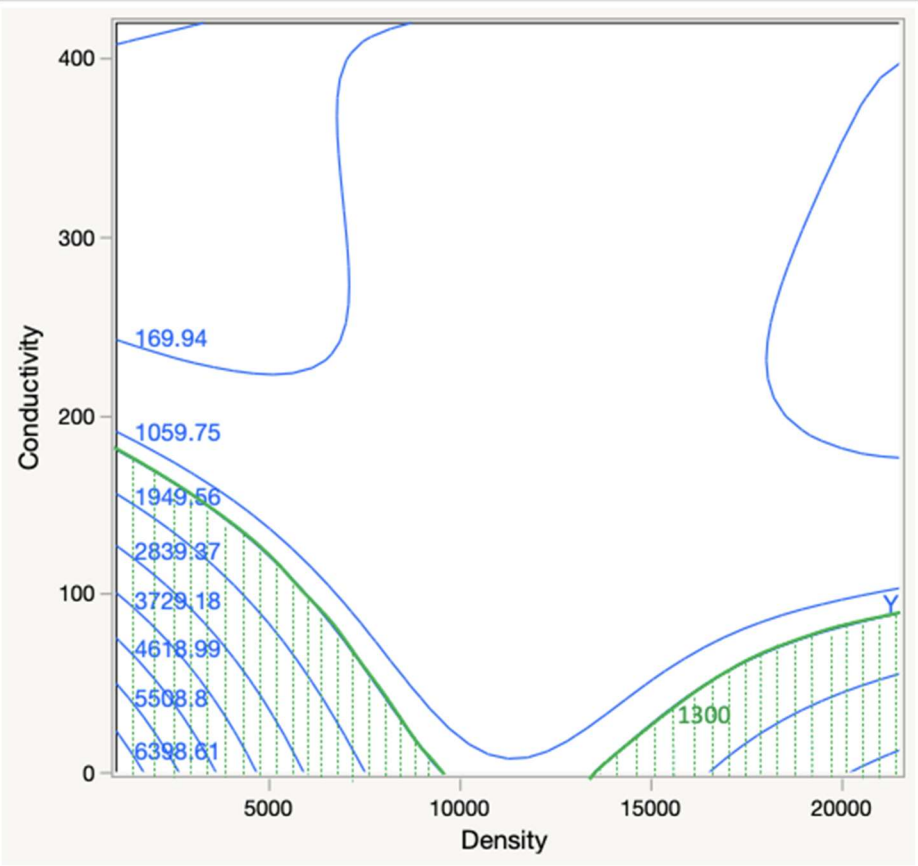

Figure 4.26. Contour profiler of Gaussian process model with shaded green optimal region. Conductivity is measured in W/(m·K) and density in kg/m^3.

4.3 Applied Materials Analysis

The located region of interest is used to identify potential real-world materials for improved slipper design. The factor space within the shaded green region of **Figure 4.26** yields a list of materials that fall within the ideal ranges for density and conductivity. These include metals, ceramics, and plastics. A list of 35 of these materials and their specifications is compiled and inputted into the Gaussian process model, which yields the estimated $\triangle T_{max}$ response. **Table 4.9** gives this list of materials, including Vascomax, in order of largest to smallest $\triangle T_{max}$. The material type is indicated by P (plastic), M (metal), or C (ceramic). This list is not exhaustive of every existing material that falls within specifications, but rather those on the market with known engineering and industrial applications.

Table 4.9. List of materials within region of interest.

Rank	**Material name, type**	**Density** g/m^3	**Conductivity** W/(m·K)	$\triangle \boldsymbol{T_{max}}$ K
1	PEI, P	1.27	0.122	5023.78438
2	PES, P	1.37	0.15	5023.05804
3	pDCPD, P	1	0.17	5022.66933
4	ABS, P	1.03	0.18	5022.41163
5	Torlon, P	1.43	0.18	5022.29378
6	PET, P	1.38	0.19	5022.05967
7	PEEK, P	1.3	0.25	5020.59035
8	PTFE, P	1.49	0.25	5020.53437
9	Nylon, P	1.14	0.27	5020.13992
10	PBT, P	1.35	0.28	5019.82928
11	POM, P	1.41	0.3	5019.31409
12	Vespel, P	1.4	0.35	5018.07339
13	Quartz, C	2.2	1.4	4991.7691
14	Ferrite, C	5	3	4951.39651
15	Zirconia, C	5.68	3	4951.19623
16	Mullite, C	2.8	4	4927.43503

17	Stainless steel, M	7.9	15	4660.701
18	FeCrAl, M	7.2	16	4637.29272
19	Silicon nitride, C	3.17	20	4544.8513
20	Titanium, M	4.5	21	4521.25973
21	Alumina, C	3.95	32	4271.69718
22	Boron carbide, C	2.52	35	4205.75321
23	Carbon steel, M	7.7	54	3801.246
24	Silicon carbide, C	3.21	60	3681.53068
25	Steel, M	7.9	80	3298.25094
26	Bronze, M	8.8	85	3207.69425
27	Nickel, M	8.8	91	3102.08083
28	Zinc, M	7.1	116	2694.65967
29	Molybdenum, M	10.2	138	2377.64879
30	Aluminum nitride, C	3.26	150	2224.19265
31	Brass, M	8.5	150	2222.64931
32	Tungsten, M	19.3	174	1944.29453
33	Cast iron, M	7.15	52	3842.41731
34	PBI, P	1.3	0.41	5016.61076
35	Platinum, M	21.4	107	2831.33161
36	Vascomax, M	8000	30.807	1409.58

The top performing materials on this list have a $\triangle T_{max}$ of approximately 256% better than the baseline Vascomax. The maximum $\triangle T_{max}$ produced from this materials list is the thermoplastic polyetherimide, or PEI (commercially sold as ULTEM®). While this material is theoretically the most promising, there are more factors than solely experimental performance to consider. One of these is cost. Since a major motivator for finding a higher performing slipper is cost effectiveness, a curve is generated to investigate which materials have the best performance to price ratio.

This cost curve is given in **Figure 4.27**. Materials on the cost efficiency frontier lie as much toward the bottom right (low cost and high $\triangle T_{max}$) as possible. The chart in part (a)

includes all 35 compiled materials; however, this chart has two materials that are so cost-prohibitive that it decreases resolution of the materials on the efficiency frontier. Part (b) eliminates these materials so that the efficiency frontier is more clearly visible. The materials on this frontier are given in **Table 4.10**.

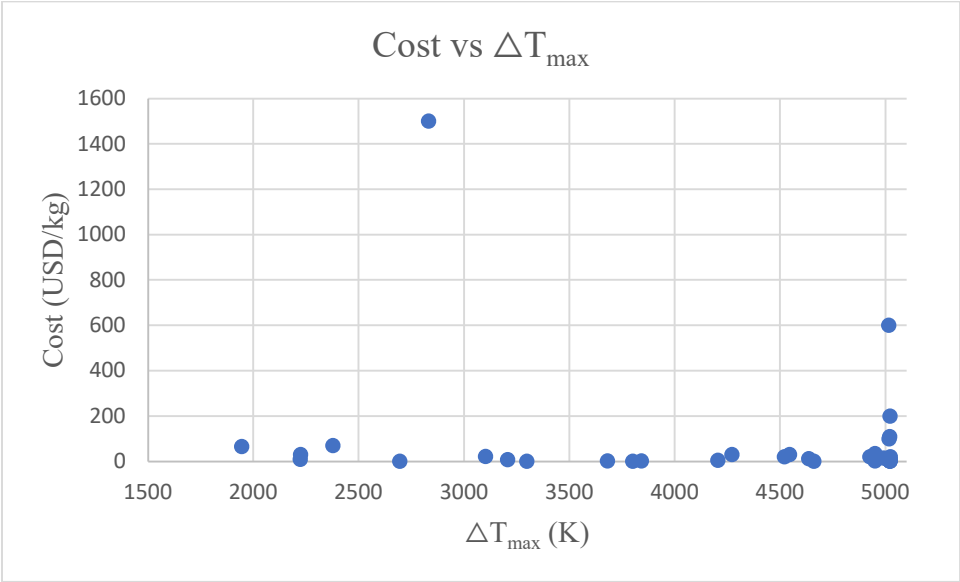

(a)

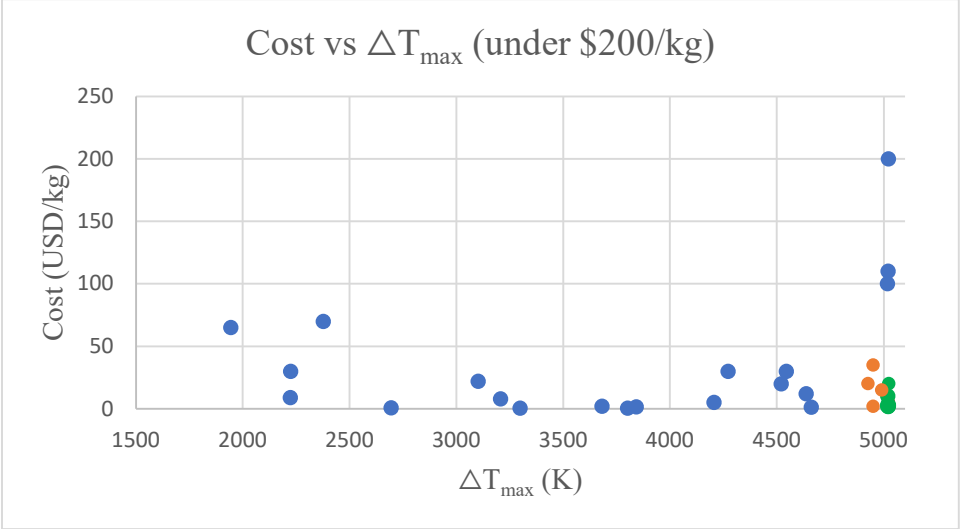

(b)

Figure 4.27. Cost vs $\triangle T_{max}$ curve of all materials (a) and materials under $200/kg (b). Points on the efficiency frontier are shown in green. Cost-effective points not on the frontier but within the resolution of the model are shown in orange.

Table 4.10. Materials on the cost efficiency frontier, in order from high to low $\triangle T_{max}$.

Material Name	**Density** g/cm^3	**Conductivity** W/(m*K)	$\triangle T_{max}$ K	**Price** USD/kg
PEI	1.27	0.122	5023.784	20
PES	1.37	0.15	5023.058	5
pDCPD	1	0.17	5022.669	3
ABS	1.03	0.18	5022.412	2
PET	1.38	0.19	5022.060	1

It is notable that all the materials on the cost efficiency frontier have very similar performance. The lowest value $\triangle T_{max}$ on the frontier is only 1.724 K less than the highest value, which is well within the estimated model error of $\pm$9.35 K as described in **Section 5.1**. Given this consideration, the most cost-effective choice on the frontier at $1/kg is the plastic polyethylene terephthalate (PET), commercially sold as Dacron®. Other cheaper materials that are not on the frontier but still perform within the bounds of optimal performance given the model's natural error is listed in **Table 4.11**. Like the materials on the efficiency curve in **Table 4.10**, these are all engineering plastics. These materials again have density and conductivity values that lie on the low end of the design space. The overall best performer considering both error and cost remains PET/ Dacron®.

Table 4.11. Cost-effective materials outside the frontier that are within optimal according to model error.

Material Name	**Density** g/cm^3	**Conductivity** W/(m*K)	$\triangle T_{max}$ K	**Price** USD/kg
PTFE/Turcite®	1.49	0.25	5020.534	10
Nylon	1.14	0.27	5020.140	2
PBT	1.35	0.28	5019.829	3
POM/Acetal	1.41	0.3	5019.314	3

Tradeoffs other than cost are also important to consider when evaluating materials. This DOE uses heat transfer as a metric for wear and experiments across the factors of density,

thermal conductivity, and specific heat. However, there are many aspects of the slipper problem not encapsulated by these metrics. For example, the highest performing materials according to the Gaussian process model are all engineering plastics. On top of performing well according to the wear model, many of these plastics are known to have advantages such as high heat and creep resistance. However, many plastics also come with issues such as being difficult to machine, low stiffness, sensitivity to ultraviolet (UV) light, and emitting toxic fumes in contact with heat or during the manufacturing process. Similarly, ceramics and metals have advantages and disadvantages that stem from the nature of their chemical composition that are not encapsulated by this experimentation. Given this, **Table 4.12** lists known pros and cons of the top three performers in each material category.

Table 4.12. Tradeoff table for top three performers in each material category in order of decreasing $\triangle T_{max}$ ("Top 5 heat-resistant plastics", "Introduction to Engineering Ceramics").

Category Rank	**Material Name**	$\triangle T_{max}$ (K)	**Cost** (USD/kg)	**Advantages**	**Disadvantages**
Plastic 1	PEI	5023.784	20	High strength and rigidity, dimensional stability over wide range of temperatures	Poor resistance to some alkali salts
Plastic 2	PES	5023.058	5	High strength and rigidity, dimensional stability over wide range of temperatures, easy fabrication	Unknown
Plastic 3	pDCPD	522.670	3	Corrosion and heat resistant, flexible molding, fast manufacturing	New material with limited known applications
Ceramic 1	Quartz	4991.769	15	Thermal shock resistant and chemical resistant	Brittle
Ceramic 2	Zirconia	4951.196	35	Corrosion and heat resistant, non-brittle, high strength and hardness, flexible fabrication options	Abrasive

Ceramic 3	Mullite	4927.435	20	High-temperature strength, thermal shock resistant, corrosion and abrasion resistant	High porosity
Metal 1	Stainless steel	4660.701	1.2	Corrosion and heat resistant, high tensile strength, easy fabrication, recyclable	Poor weldability (ferritic and martensitic)
Metal 2	FeCrAl	4637.297	12	Corrosion and heat resistant	Brittle
Metal 3	Titanium	4521.260	20	Corrosion resistant, high strength, abundant	High reactivity that causes difficult manufacturing, environmentally destructive extraction

V. Model Validation

This DOE is conducted with a computer-simulated representation of the pin-on-disc experiment. As such, it is important to examine whether this model accurately represents the true behavior of the physical experiment. One major downfall to the FEA model is that it is built off of a single experimental run from 2019. Because the FEA is only calibrated to this one observational temperature profile, it is unknown whether the model truly represents the experiment. This section of research statistically analyzes whether the model is a good representation of the physical wear event on the pin-on-disc rig.

5.1 Test Process

While the FEA model suitably represents the 2019 experimental run, it is unknown whether this run is representative of true temperature behavior. As such, additional tests were conducted at the AFRL Aerospace Systems Directorate's (AFRL/RQ) pin-on-disc rig. These runs are analyzed and statistically compared with the 2019 run.

The setup and test plan of these runs reproduce those of the original 2019 run as closely as possible. The rig's basic design and functionality are as specified in **Section 2.2**. The rig components that perform the wearing event and the measurement devices remain largely the same as the old design, as shown in **Figure 5.1**. This includes the 12-inch AISI 4340 steel disc, the Vascomax®300 pin, motor-actuated holder, and position sensor. The three thermocouples are embedded into the specimen in the same manner as specified in **Section 2.2**, but type K thermocouples with a maximum temperature threshold of 1530 K are used instead of the old type J (maximum 1030 K). A schematic of the full system used in the 2021 test is given in **Figure 5.2** (Walter).

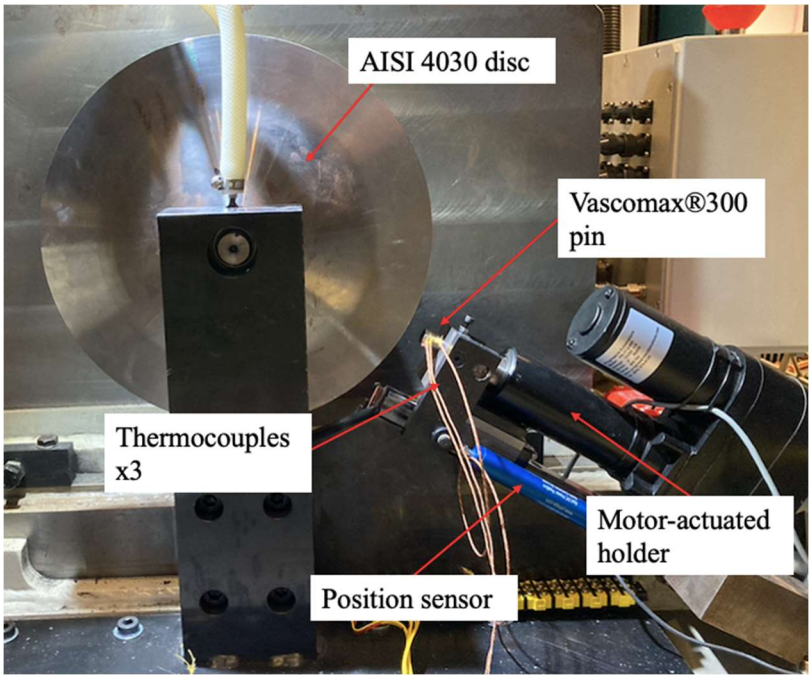

Figure 5.1. 2021 pin-on-disc rig.

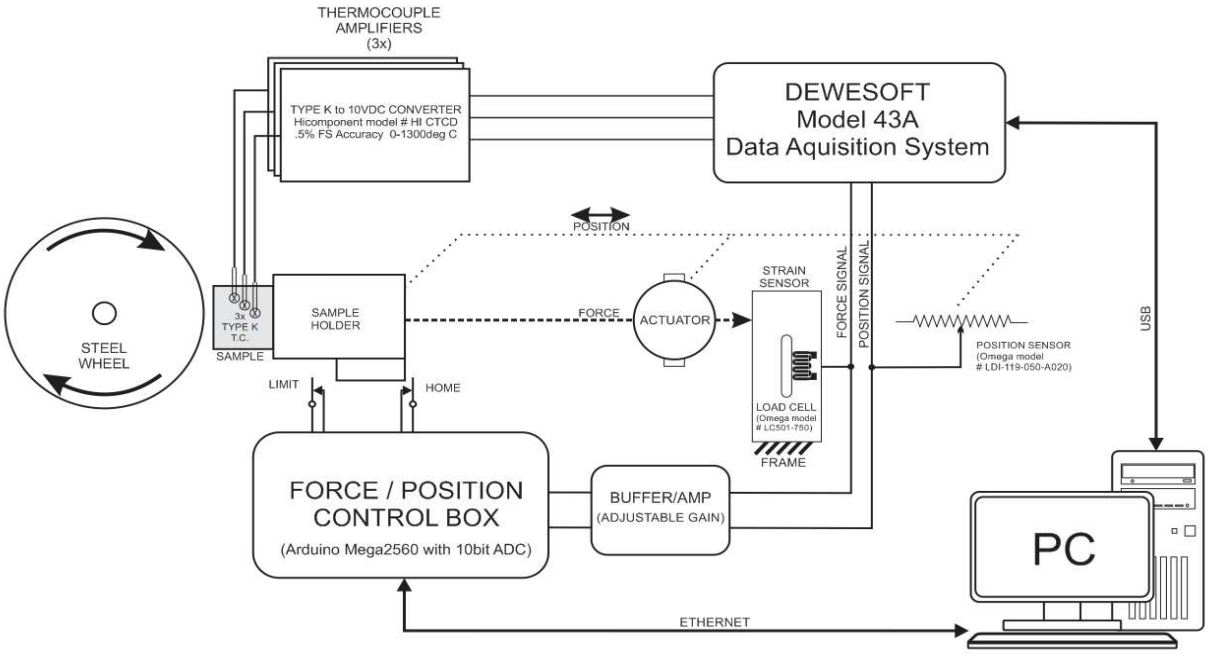

Figure 5.2. Schematic of the 2021 pin-on-disc system (Walter).

To run the system, an operator specifies the run time of the wearing event using the PC. The operator also specifies the force to be applied between the pin and the spinning AISI 4340 steel wheel, as shown in **Figure 5.2**'s PC to force control box interface. The force controller

operates with a feedback loop that senses the force and adjusts accordingly. This update is performed every 18 degrees of wheel revolution. The desired velocity of the wheel in rotations per minute (RPM) is also inputted via an external controller. The values used for the run time, force, and velocity are given in **Table 5.1**. During the entire run time, the three thermocouples embedded in the specimen pin capture the temperature inside the pin and send the data to the DEWESOFT data acquisition box. A total of nine validation runs are performed with this system.

There is measurement error associated with the rig system. The error on the Type K thermocouples is the maximum of 2.2 K and 0.75% of the measurement. In other words, measurements under approximately 300 K have an error of $\pm$0.75% while measurements over 300 K have an error of $\pm$2.2 K. The thermocouple amplifier has an error of $\pm$0.5%, which is approximately $\pm$6.5 K at maximum temperature. The DEWESOFT data acquisition box has an error of $\pm$0.65 K according to the manufacturer. Therefore, the maximum error on this system is the sum of errors, or $\pm$9.35 K. This value is important to consider when comparing the performance of alternatives as in **Section 4.3**. Because the FEA temperature profile is based off these measurements, this error also applies to model temperature outputs.

Despite the goal to reproduce original operating conditions to perform data validation, there are a few differences between the 2019 run and the newer tests. In terms of system function, the older test applies the pin to the rig using a human-in-the loop method whereas the new system is closed-loop once the wearing event begins. In the 2019 setup, an engineer presses a button to move the pin holder forward as the run proceeds and the pin wears down. The 2021 setup uses a sensor-operated system that applies a near-constant force over the duration of the run. This updated setup is necessary because it is difficult for a human to control the amount of

force applied in the high-speed pin-on-disc environment. It would be nearly impossible for a human operator to manually reproduce the same force profile as applied in 2019 over the course of several replicated runs. Therefore, a machine-controlled system is used to replicate the 2019 run with as much fidelity as possible.

Another difference between the 2019 and 2021 runs is the diameter of the pin. The older Vascomax pins have a diameter of 0.55 inches, while the newer pins are manufactured with a diameter of 0.50 inches. This is significant because the area of the pin A is inversely proportional to surface heat flux as in equation (3), and thus to heat transfer-induced wear. Equation (3) shows that F and A are also inversely proportional to each other, so the applied force F must be adjusted to reproduce operating conditions as much as possible. The following relationship is used to calculate the corrected force:

$$\frac{F_{old}}{A_{old}} = \frac{F_{new}}{A_{new}} \tag{5}$$

where A is given by $\pi(D/2)^2$, D being the diameter of the pin face. Using the old and new D values of 0.55 and 0.50 respectively, equation (5) gives that $F_{old} = 0.8264F_{new}$. Given this correction, 2021 test parameters are adjusted according to **Table 5.1**. Parameters marked with an asterisk (*) indicate discrepancy between the old and newer tests. Values are given in both scientific units and the units inputted into the rig system software. Note that velocity is converted to rotations per minute (RPM) given the diameter of the 12-inch AISI 4340 wheel.

Table 5.1. 2019 vs 2021 test parameters.

Test parameter	2019 SI	2019 Field	2021 SI	2021 Field
$F*$	656.76 N	148 lbf	542.75 N	122 lbf
v	47.83 m/s	3000 RPM	47.83 m/s	3000 RPM
$A*$	0.00015328 m^2	0.55 in	0.0001267 m^2	0.50 in
Run time	9 s	9 s	9 s	9 s

5.2 Validation Analysis

The temperature profiles from the 9 validation runs are analyzed and compared to the temperature profile generated by the FEA model. The goal is to determine whether the collected data supports the model output. The variable tested in this analysis is the response, $\triangle T_{max}$, which is measured from the temperature profile of each run as specified in **Section 4.1.1**. An example temperature profile taken from a validation run is shown in **Figure 5.3**. The sample mean of these 9 runs is $\bar{y} = 1038.429$ K with sample standard deviation $s = 68.396$ K. The corresponding model temperature profile is generated using the FEA, with flux adjusted according to the new values of F and A given in **Table 5.1**. Plugging these diameter-corrected values into equation (3) gives a flux of $4.918 \cdot 10^6 \frac{W}{m^2}$ compared to the old flux of $5.950 \cdot 10^6 \frac{W}{m^2}$. The resulting temperature profile is given in **Figure 5.4**, with a $\triangle T_{max}$ of 1167.170 K.

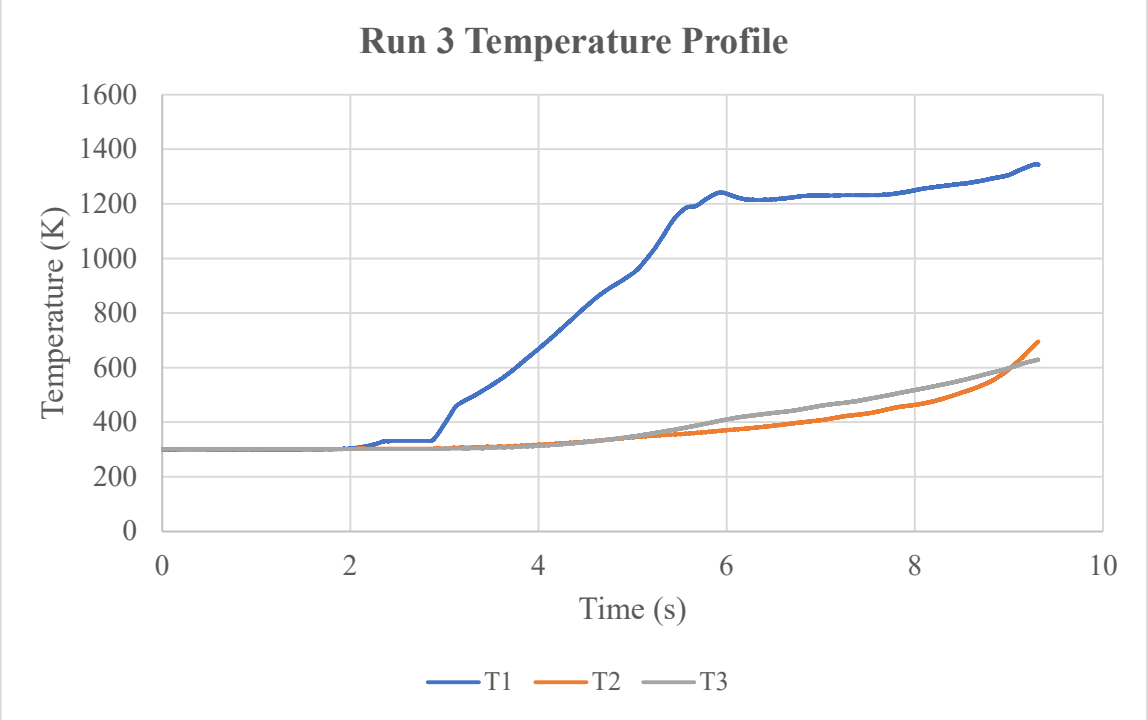

Figure 5.3. Example temperature profile from 2021 validation run #3. $\triangle T_{max}$ for this run is calculated as $\triangle T_{max} - T_0 = 1344.297 - 300.569 = 1043.727K$.

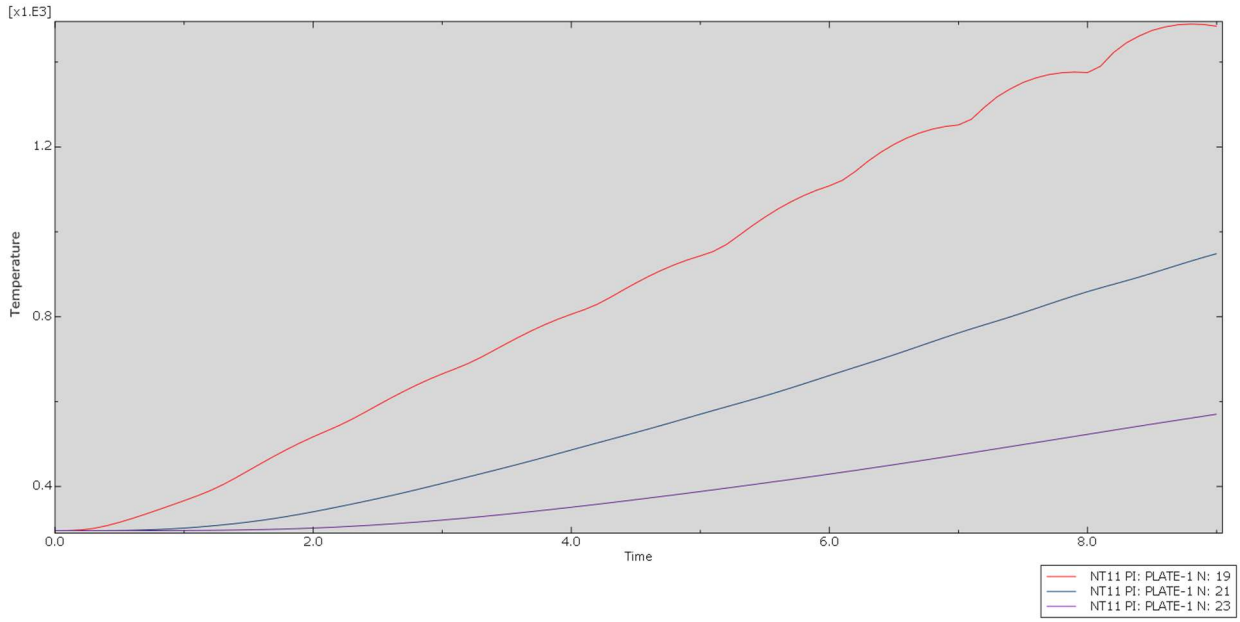

Figure 5.4. Temperature profile generated from the FEA using the adjusted flux model.

The FEA-generated temperature profile is compared with those of the physical runs to determine if the model is supported by test data. To do this, the model $\triangle T_{max}$ is compared with the true mean as estimated from the test runs. This is accomplished by constructing a two-sided 95% confidence interval around the mean. A t-distribution is used to construct the interval, which yields a range between 985.855 and 1091.003 K. As the model $\triangle T_{max}$ of 1167.170 K lies outside this range, it is concluded that the model likely does not represent the true mean of the pin-on-disc experiments.

In addition to examining whether the model is reflective of the true mean, outlier analysis can be performed to test whether the model lies within the distribution of $\triangle T_{max}$ at all. As there is no one method of using sample data to determine whether a data point lies within the population distribution, this is tested with a variety of statistical techniques: the prediction interval, normal probability plot, Grubbs' outlier test, and outlier box plot.

A prediction interval provides a range of values that a single future observation may fall under. The two-sided 95% prediction interval of the test data is [872.175 K, 1204.682 K]. As the

model $\triangle T_{max}$ of 1167.170 K falls within this range, the prediction interval affirms that the model output likely lies within the distribution of the pin-on-disc experiment. This conclusion is supported by the normal probability plot in **Figure 5.5**, which shows that the model output (labelled as the red data point) lies within the dotted red band of approximately normally distributed data. An outlier would likely fall outside this band. The histogram shown on the left of **Figure 5.5** confirms this approximately normal behavior.

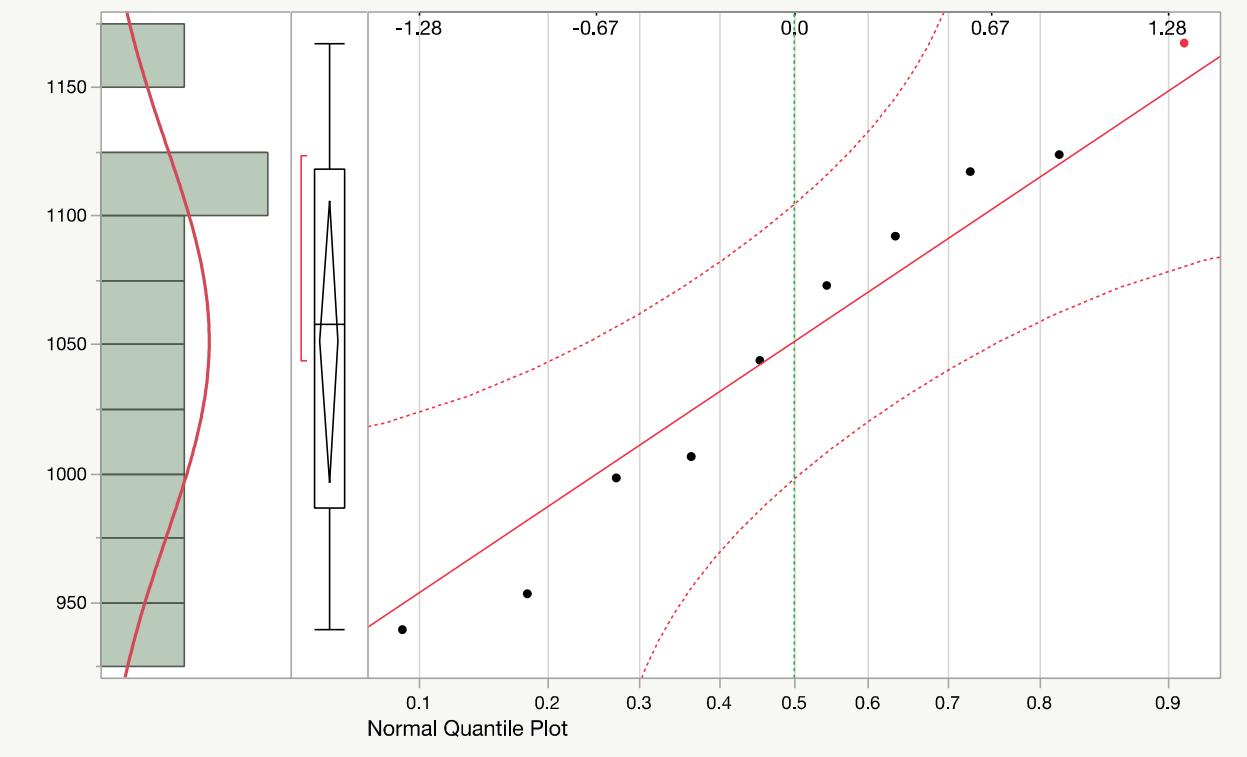

Figure 5.5. Graphical descriptions of the dataset from left to right: histogram, outlier box plot, and normal probability plot.

An underlying normal distribution is useful so that formal outlier tests may be performed. These tests depend on the assumption of normality. Grubbs' outlier test detects whether there is a single outlier in a dataset, with the null hypothesis being that there are no outliers and the alternative that there is exactly one. The test statistic G is defined as:

$$G = \frac{max|y_i - \bar{y}|}{s} \tag{5}$$

where y_i is the i^{th} observation, $\bar{y}$ is the sample mean, and s is the sample standard deviation. The G value of the test data is 1.519, which is below the critical level of 2.290. This indicates failure to reject the null hypothesis. Therefore, none of the data points, including the model-generated point, are considered outliers. The final test to confirm this is **Figure 5.5**'s outlier box plot, in which the model data point of 1167.170 K lies on the "whisker" of the plot, not outside the range. In summary, statistical analysis shows that while the model output likely lies within the experimental distribution, it likely does not represent the true mean.

In addition to this statistical conclusion, the FEA model has several process-based limitations. For one, the model incorrectly uses a pin diameter of 0.50 inches when the pin from 2019 has a diameter of 0.55 inches. Although the FEA closely represents the 2019 thermal profile despite this error, there are likely modeling inconsistencies that impact thermal profiles when experimenting across the material design space. Another issue that could affect the accuracy of DOE results is the use of constant parameters in the heat flux equation (3). While these parameters again suffice to represent the 2019 run, heat flux is known to be a time variable property. These issues suggest that experimental results should be used with caution for use in future testing. A future recommendation is to construct a new model based off of the full test data and information acquired in 2021. The FFFD designed in **Section 4.2.2** should then be applied to this updated wear model for a more reliable experimentation.

VI. Conclusion

This work uses experimental design to mathematically characterize the behavior of high-speed wear due to heat transfer. Experimentation in this research is conducted on the 1D transient FEA representation of AFRL's pin-on-disc experiment. The most appropriate design for this problem is the FFFD, given the irregular shape of the design space. A total of 21 design points are tested using an augmented FFFD, with the baseline Vascomax performing in the 77^{th} percentile of all observations.

Of the resulting models that are generated from this design, it is determined that the Gaussian process model is the most accurate due to the highly nonlinear behavior of wear. The Gaussian process model estimates that the factor of material conductivity has the highest impact on the $\triangle T_{max}$ response with a total sensitivity value of 0.866. Density is also a significant predictor to the response, while the impact of specific heat is negligible. A significant portion of sensitivity also comes from the interaction between conductivity and density, with a value of 0.336.

The Gaussian process model produces a response profile that can be used to identify the region in the factor space that generates a $\triangle T_{max}$ that is at or greater than the baseline Vascomax slipper material. This yields a list of commercially available materials that fall within these specifications. According to the model, the highest performing materials are all engineering plastics. Cost analysis is performed to identify materials on the efficiency frontier of price and performance. The overall best performer considering cost and the margin of model error is the engineering plastic PET (Dacron®). High-performing materials according to the model are also assessed in regard to aspects such as malleability, impact resistance, and ease of manufacturing.

This work concurrently performs model validation on the 1D FEA of the pin-on-disc experiment. Nine additional runs are performed at AFRL/RQ, which yield that the current FEA

likely falls within the distribution of maximum thermal output, but that it likely does not represent the true mean. In addition, micromechanical analysis of worn pin specimens indicate that significant wear is induced from mechanical stress. This wear, which includes plastic deformation and potential additional thermal effects, is not accounted for by heat transfer. As such, the experimentation in this research provides materials that wear ideally according to solely a heat transfer perspective.

This research provides a proof of concept for using experimental design to mitigate high-speed sliding wear. Potential future work in this field involves direct materials experimentation using the pin-on-disc rig. The findings of this research demonstrate the need for physical experimentation in a controlled setting that mimics the high speed, temperature, and force conditions of the HHSTT. Existing models and simulations provide valuable information on certain characteristics of slipper wear behavior such as heat transfer. However, they cannot holistically represent all possible wearing behavior, and have issues extrapolating outside the immediate scope of the model.

Recommendations for further research include using the methods, data, and insight provided by this work to construct, conduct, and analyze a physical DOE at AFRL/RQ's pin-on-disc rig. This involves selecting appropriate response variable(s) and design space. Unlike simulated experimentation, points should be replicated to estimate pure error. For fitting a model, a Gaussian process model is recommended due to the observed highly nonlinear behavior of wear.

Bibliography

"846th Test Squadron Holloman High Speed Test Track." *Holloman Air Force Base*, www.holloman.af.mil/About/Units/704th-Test-Group/846-TS/. Accessed 1 Jun. 2021.

Ayers, Kevin. "First Plastics, Then Metals and Now Composites." *SME*, 10 May 2017, www.sme.org/technologies/articles/2017/may/first-plastics-then-metals-and-now-composites/.

Bayer, Raymond. *Engineering Design for Wear*, 2nd ed., New York, CRC Press, 2004.

Bergman, Theodore, et al. *Fundamentals of Heat and Mass Transfer*, 7th ed., Hoboken, John Wiley & Sons, 2011.

Boardman, Brian. *Modeling Nonlinear Heat Transfer for a Pin-on-Disc Sliding System*. 2020. Air Force Institute of Technology, Master's Thesis.

"Engineering Plastics." *AcmePlastics*, www.acmeplastics.com/engineering-plastics. Accessed 1 Nov. 2021.

Gerstle, Frank, et al. "Thermoplastic shear and fracture of steel during high-velocity sliding." *Wear*, vol. 24, no. 1, 1973, pp. 97-106.

Gregersen, Erik. "Thermal Conduction." *Britannica*, 7 Feb. 2018, www.britannica.com/science/thermal-conduction.

Hooser, Michael. Personal interview. 1 Aug. 2021.

Hutchings, Ian. *The Challenge of Wear*. Chichester, John Wiley & Sons, 2005.

"Gaussian Process Fit Data Using Smoothing Models." *jmp*, www.jmp.com/support/help/en/16.1/index.shtml#page/jmp/gaussian-process.shtml#. Accessed 1 Oct. 2021.

"Internal Energy." *hyperphysics,* hyperphysics.phy-astr.gsu.edu/hbase/thermo/inteng.html#c2. Accsesed 1 Oct. 2021.

"Introduction to Engineering Ceramics." *Great Ceramic,* 19 Jan. 2021, great-ceramic.com/introduction-to-engineering-ceramics/.

Jones, Bradley and Ryan Lekvietz. "Fast Flexible Filling in Space Filling Designs." *JMPer Cable*, 2014, pp. 5-8.

Lim, Seh Chun and Michael Ashby. "Wear Mechanism Maps." *Acta Metallurgica*, vol. 35, 1987, pp. 1-24.

Liu, Bert. "Microstructural Analysis of High-Speed-Wear (Pin-on-Disc) Test Samples." 14 May 2019.

"Metal properties table." *Tibtech*, 2018, www.tibtech.com/conductivite. Accessed 1 Oct. 2021.

Montgomery, Douglas. *Design and Analysis of Experiments*, 9th ed., Hoboken, John Wiley & Sons, 2017.

Muhamed, Melisa. "[Mastering JMP] Response Surface Methods for Optimization." *jmp*, 3 Sep. 2020, community.jmp.com/t5/Melisa-Muhamed-s-Blog/Mastering-JMP-Response-Surface-Methods-for-Optimization/ba-p/299177.

Rivière, Lisa, et al. "Specific heat capacity and thermal conductivity of PEEK/Ag nanoparticles composites determined by Modulated-Temperature Differential Scanning Calorimetry." *Polymer Degradation and Stability,* vol. 127, 2016, pp. 98-104.

Szmerekovsky, Andrew. *The Physical Understanding of the Use of Coatings to Mitigate Hypervelocity Gouging Considering Real Test Sled Dimensions*. 2004. Air Force Institute of Technology, PhD dissertation.

"Thermal Conductivity Easily Transmits Heat." *Kyocera*, global.kyocera.com/fcworld/charact/heat/thermalcond.html. Accessed 1 Oct. 2021.

"Top 5 heat-resistant plastics." *Fast Radius*, www.fastradius.com/resources/top-5-heat-resistant-plastics/. Accessed 1 Nov. 2021.

Walter, Laura. "WOD Equipment and Error." 17 Dec. 2021. *Air Force Research Laboratory, Aerospace Systems Directorate*. Lab manual.

Williams, Jim. "The science and technology of composite materials." *Australian Academy of Science,* 18 Jun. 2015, www.science.org.au/curious/technology-future/composite-materials.

Wing, Aron. *Modeling a High Speed Pin-on-Disc Experiment by Comparison of Numerical Solutions to a Moving Boundary Nonlinear Heat Equation*. 2021. Air Force Institute of Technology, Master's thesis.

Worley, Bill. "Case Study – The Use of Gaussian Process for Analyzing Computer Generated Experiments." *jmp*, 13 Nov. 2020, community.jmp.com/t5/Discovery-Summit-Korea-2020/Case-Study-The-Use-of-Gaussian-Process-for-Analyzing-Computer/ta-p/333321.

Yeo, Chang-Dong, et al. "Evaluation of Thermomechanical Damage of a Slipper and Rail in a Rocket Sled System." *Journal of Testing and Evaluation,* 2016, www.researchgate.net/publication/282453935_Evaluation_of_Thermomechanical_Damage_of_a_Slipper_and_Rail_in_a_Rocket_Sled_System.

REPORT DOCUMENTATION PAGE

Form Approved
OMB No. 0704-0188

1. REPORT DATE *(DD-MM-YYYY)*	2. REPORT TYPE	3. DATES COVERED *(From - To)*
24-03-2022	Master's Thesis	September 2020 - March 2022

4. TITLE AND SUBTITLE
Experimental Design on High-Speed Sliding Wear

5a. CONTRACT NUMBER

5b. GRANT NUMBER

5c. PROGRAM ELEMENT NUMBER

6. AUTHOR(S)
Liew, Irene D., 2d Lt, USAF

5d. PROJECT NUMBER

5e. TASK NUMBER

5f. WORK UNIT NUMBER

7. PERFORMING ORGANIZATION NAME(S) AND ADDRESS(ES)
Air Force Institute of Technology
Graduate School of Engineering and Management (AFIT/EN)
2950 Hobson Way
Wright-Patterson AFB OH 45433-7765

8. PERFORMING ORGANIZATION REPORT NUMBER
AFIT-ENS-MS-22-M-145

9. SPONSORING/MONITORING AGENCY NAME(S) AND ADDRESS(ES)
Dr. Russell Spyker
1950 5th St., Bldg 18B Rm 15
Air Force Research Laboratory, Aerospace Systems Directorate
WPAFB, OH 45433
russell.spyker.1@us.af.mil

10. SPONSOR/MONITOR'S ACRONYM(S)
AFRL/RQ

11. SPONSOR/MONITOR'S REPORT NUMBER(S)

12. DISTRIBUTION/AVAILABILITY STATEMENT
DISTRIBUTION STATEMENT A:
APPROVED FOR PUBLIC RELEASE; DISTRIBUTION UNLIMITED.

13. SUPPLEMENTARY NOTES

14. ABSTRACT
The purpose of this research is to develop, conduct, and analyze an experimental design that characterizes wear rates of various materials sliding at high speeds along an AISI 4340 steel rail. This work is in support of Holloman Air Force Base, which is invested in engineering a more wear-resistant rocket slipper for its high-speed test track. This research uses a design of experiments approach to systematically identify and evaluate potential slipper attributes that mitigate wear according to a heat transfer model. Final findings include recommendations of slipper materials that theoretically perform similar to or better than the baseline Vascomax®C300 maraging steel material. Concurrently, this research statistically

15. SUBJECT TERMS
Experimental Design, Design of Experiments, High-Speed Wear, Pin-on-Disc, Holloman High Speed Test Track

16. SECURITY CLASSIFICATION OF:			17. LIMITATION OF ABSTRACT	18. NUMBER OF PAGES	19a. NAME OF RESPONSIBLE PERSON
a. REPORT	b. ABSTRACT	c. THIS PAGE			Dr. Raymond R. Hill, AFIT/ENS
U	U	U	UU	100	19b. TELEPHONE NUMBER *(Include area code)*: 937-255-6565 x7469; raymond.hill@afit.edu